Materials Today Bio 32 (2025) 101810

Contents lists available at ScienceDirect

Materials Today Bio

journal homepage: www.journals.elsevier.com/materials-today-bio

A novel hydrogel loaded with plant exosomes and stem cell exosomes as a new strategy for treating diabetic wounds

Jialu Weng [a,d,1], Yizhang Chen [d,f,1], Yuhan Zeng [a,d,f,1], Wenzhang Jin [a,b,d,*,1], Ying Ji [e], Wa Zhang [b,d], Shunfu Wang [a,d], Haobing Li [d], Meilin Yi [d], Xiaoying Niu [d], Xuchen Deng [d], Jiancheng Huang [e,**], Xiang Su [a,c,***], Lulu Chen [a,c,****]

[a] Department of Anesthesia, The First Affiliated Hospital of Wenzhou Medical University, Wenzhou, 325000, PR China
[b] Department of Colorectal Surgery, The Second Affiliated Hospital of Zhejiang Chinese Medical University, Hangzhou, 310000, PR China
[c] Department of Vascular Surgery, The First Affiliated Hospital of Wenzhou Medical University, Wenzhou, 325000, PR China
[d] Key Laboratory of Diagnosis and Treatment of Severe Hepato-Pancreatic Diseases of Zhejiang Province, The First Affiliated Hospital of Wenzhou Medical University, Wenzhou, 325000, PR China
[e] Department of Nephrology, The First Affiliated Hospital of Ningbo University, Ningbo, 315010, PR China
[f] School of Pharmaceutical Sciences, Wenzhou Medical University, Wenzhou, 325000, PR China

ARTICLE INFO

Keywords:
Momordica charantia
Mesenchymal stem cell
Exosomes
Hydrogel
Diabetic wounds

ABSTRACT

Diabetic wound healing is constrained by various factors, including chronic inflammation, sustained oxidative stress, impaired angiogenesis, and abnormal wound microenvironments. Exosomes derived from mesenchymal stem cells (MSC-exo) contain a wealth of bioactive substances that play a positive role in promoting diabetic wound healing. Plant-derived exosomes, as a novel therapeutic approach, are continuously being explored. Momordica charantia (MC) has been shown to possess blood glucose-lowering effects, and its exosomes are of significant relevance for treating diabetic wounds. However, direct application of exosomes to wounds faces challenges such as poor stability and short retention time, limiting their therapeutic effectiveness and clinical applicability. Encapsulating exosomes in hydrogels is an effective strategy to preserve their bioactivity. In this study, we fabricated a hydrogel loaded with MSC-exo and MC exosomes (MC-exo) by photopolymerization of methacrylated gelatin (GelMA) and dopamine (MEMC-Gel). The resulting MEMC-Gel exhibited favorable mechanical properties, adhesion, degradability, absorbency, and biocompatibility. In vitro, MEMC-Gel demonstrated the ability to resist inflammation, counter oxidative stress, promote fibroblast migration, support endothelial cell angiogenesis, and regulate macrophage polarization. In a diabetic mouse wound model, MEMC-Gel accelerated wound healing by inhibiting inflammation and oxidative stress, modulating macrophage immune responses and hyperglycemia within the microenvironment, promoting angiogenesis, and enhancing epithelialization. In conclusion, MEMC-Gel is an outstanding hydrogel dressing that synergistically promotes repair by loading MSC-exo and MC-exo, significantly accelerating diabetic wound healing through multiple mechanisms. This multifunctional hydrogel, based on exosomes from two different sources, provides an innovative therapeutic strategy for diabetic wound repair with broad clinical application potential.

1. Introduction

Diabetic wounds, particularly diabetic foot ulcers, are a severe complication of diabetes and often lead to serious consequences such as infections, amputations, and even death [1]. The characteristics of diabetic wounds are multifactorial, including hyperglycemia, neuropathy, excessive oxidative stress, poor circulation, and chronic inflammation, all of which collectively hinder the healing process [2–4].

* Corresponding authors. Department of Colorectal Surgery, The Second Affiliated Hospital of Zhejiang Chinese Medical University, Hangzhou, 310000, PR China.
** Corresponding author. Department of Nephrology, The First Affiliated Hospital of Ningbo University, Ningbo, 315010, PR China.
*** Corresponding authors. Department of Vascular Surgery, The First Affiliated Hospital of Wenzhou Medical University, Wenzhou, 325000, PR China.
**** Corresponding author. Department of Anesthesia, The First Affiliated Hospital of Wenzhou Medical University, Wenzhou 325000, PR China.
E-mail addresses: 228927178@qq.com (W. Jin), hjczju@hotmail.com (J. Huang), 43737136@qq.com (X. Su), 13732059853@163.com (L. Chen).
[1] These authors contributed equally to this work.

https://doi.org/10.1016/j.mtbio.2025.101810
Received 26 January 2025; Received in revised form 8 April 2025; Accepted 26 April 2025
Available online 27 April 2025

Hyperglycemia has multiple detrimental effects on wound healing. It promotes the formation of advanced glycation end products (AGEs), which exacerbate oxidative stress and inflammation, further impairing the healing process [5,6]. Excessive oxidative stress is another major factor contributing to impaired wound healing in diabetic patients [7]. This oxidative stress damages cellular structures, proteins, and DNA, leading to further complications during the healing process [8]. Poor blood circulation, often a result of diabetes-related vascular complications, limits the delivery of essential nutrients and oxygen to the wound site [9]. This insufficiency slows the healing process and increases the risk of infection [10]. Chronic inflammation is also a critical barrier to diabetic wound healing. Persistent release of pro-inflammatory cytokines due to chronic inflammation further damages tissues and delays the healing process. In diabetic-related wounds, immune response dysfunction in the local microenvironment has been identified as a core mechanism contributing to excessive inflammatory responses [11–13]. Macrophages, one of the most important immune cells in wound healing, have their immune function severely impaired in the diabetic wound microenvironment, affecting the healing process [14]. Currently, treatments for diabetic wounds face numerous limitations. Conventional dressings, traditional herbal applications, surgical debridement, and antibiotic therapies often fail to effectively address these issues, leading to infections and delayed healing [15–17]. Numerous innovative therapies, such as antioxidant hydrogels, scaffolds, microneedles, hydrogels, and multifunctional biomaterials, are being explored [18–20]. Overall, there is an urgent need for more effective treatment strategies for diabetic wound management.

Exosomes are small extracellular vesicles, typically ranging from 30 to 150 nm in diameter. They play a crucial role in intercellular communication by transferring proteins, lipids, and nucleic acids between cells [21]. This molecular signaling can influence the behavior of recipient cells, making exosomes a key focus of research in regenerative medicine and therapeutic applications [22]. In the context of wound healing, exosomes have gained attention for their potential to accelerate both acute and chronic wound repair. For instance, exosomes derived from human umbilical cord blood have been shown to promote fibroblast function, angiogenesis, and M2 macrophage differentiation [23], all of which are key processes vital for wound healing. The application of exosomes in wound healing is not limited to their natural form, as bioengineering strategies have been employed to enhance their therapeutic properties. For example, exosomes can be incorporated into materials such as hydrogels to provide a controlled release system, improving their stability and retention at the wound [24], thereby enhancing their effects on wound closure and tissue regeneration.

Exosomes derived from stem cells, particularly those from mesenchymal stem cells (MSC), have shown tremendous potential in promoting wound healing due to their ability to modulate inflammation, stimulate angiogenesis, and promote tissue regeneration [25]. These vesicles carry bioactive molecules that influence various stages of wound healing, including the proliferation and migration of fibroblasts and keratinocytes, which are crucial for tissue repair [26]. MSC-derived exosomes (MSC-exo) have demonstrated significant promise as an acellular therapeutic tool in chronic wound healing [27].

Plant-derived exosomes, a growing field of research in plant biology and medicine, also hold considerable potential for wound healing applications [28,29]. Momordica charantia (MC) has garnered attention for its anti-inflammatory, antioxidant, and blood glucose-lowering properties [30,31]. Studies have shown that MC extracts significantly inhibit the expression of pro-inflammatory genes, demonstrating potent anti-inflammatory effects that may aid in managing inflammatory diseases [32]. Additionally, cucurbitane compounds in MC have been shown to downregulate the expression of pro-inflammatory factors such as NF-κB and iNOS, further supporting its anti-inflammatory potential [33,34]. MC also exhibits blood glucose-lowering effects [35], and research on type 2 diabetes mouse models suggests that it can improve body weight, blood glucose levels, and insulin sensitivity [36]. The bioactive compounds in MC contribute to reducing oxidative stress [37]. Based on these findings, it is hypothesized that MC-derived exosomes (MC-exo) could have therapeutic potential in wound healing, offering a novel strategy for treating diabetic wounds. By harnessing the rich bioactive compounds within MC-exo, future research could support the development of innovative plant-based therapies to address wound healing and metabolic disorders, ultimately improving patient outcomes and quality of life.

In recent years, hydrogels have attracted significant attention as wound dressings [38]. Methacrylated gelatin (GelMA) hydrogels, due to their excellent biocompatibility and mechanical properties, have become an ideal material for wound dressings [39]. Introducing dopamine (DA) into hydrogels can enhance their adhesive properties [40,41], further improving their potential for wound healing applications. Additionally, hydrogels can serve as carriers for exosomes [42], providing sustained release of bioactive molecules while modulating the wound microenvironment to promote tissue regeneration and repair.

In this study, we used GelMA and DA as materials to embed MSC-exo and MC-exo into a hydrogel (Fig. 1A), aiming to develop a novel exosome-enhanced hydrogel dressing loaded with both stem cell and plant-derived exosomes (MEMC-Gel) to enhance diabetic wound healing and repair. Experimental results indicate that MEMC-Gel not only exhibits good mechanical strength, adhesion, and biocompatibility, but it also improves the wound microenvironment by regulating the inflammatory response, combating oxidative stress, promoting angiogenesis, modulating blood glucose levels, and adjusting macrophage immune responses, thereby accelerating wound healing (Fig. 1B). In conclusion, a novel multifunctional hydrogel, MEMC-Gel, was successfully developed, showing great potential in promoting diabetic wound healing, tissue regeneration, and wound repair.

2. Materials and methods

2.1. Materials

Fresh momordica charantia (MC) was purchased from a local grocery store (Wenzhou, China), gelatin, methacrylic anhydride, dopamine hydrochloride (DA), and lithium phenyl-2,4,6-trimethylbenzoylphosphinate (LAP), type II collagenase were purchased from Sigma-Aldrich (St. Louis, USA). BCA Assay Kit, Radio immunoprecipitation assay (RIPA), RNA Isolation Kit, Calcein AM, reactive oxygen species (ROS) assay kit, and Cell Counting Kit-8 (CCK-8) were purchased from Beyotime (Shanghai, China). $NaHCO_3$ and the ROS fluorescent probe dihydroethidium (DHE) were purchased from Aladdin (Shanghai, China). Polyethylene glycol 8000 (PEG8000), Triton X100, streptozotocin (STZ), lipopolysaccharide (LPS), sodium citrate buffer, and 4 % paraformaldehyde were obtained from Solarbio (Beijing, China). The red fluorescent tracing reagents for exosomes (PKH26, PKH67) were obtained from Yeasen (Shanghai, China). Dulbecco's Modified Eagle Medium (DMEM), RPMI 1640 medium, fetal bovine serum (FBS), phosphate-buffered saline (PBS), and trypsin-EDTA were all obtained from Thermo Fisher Scientific (Waltham, USA). Matrigel matrix was purchased from Corning (Corning, USA). Recombinant Anti-CD9 antibody (ab307085), recombinant Anti-CD81 antibody (ab109201), recombinant Anti-CD63 antibody (ab315109), recombinant Anti-CD31 antibody (ab182981), recombinant Anti-iNOS antibody (ab178945), and recombinant Anti-Mannose Receptor (CD206) antibody (ab300621) were purchased from Abcam (Cambridge, UK). Myeloperoxidase (MPO) Rabbit polyclonal antibody (A1374) and AGER Rabbit monoclonal antibody (A23422) were obtained from Abclonal (Wuhan, China). Mouse TNF-α ELISA kit, Mouse IL-1β ELISA kit, Mouse IL-6 ELISA kit, Mouse IL-10 ELISA kit, Mouse VEGF ELISA kit, and Mouse TGF-β1 ELISA kit were purchased from MultiSciences Biotech Co., Ltd (Hangzhou, China). Hydroxyl free radical (·OH) assay kit, Superoxide dismutase (SOD) assay kit (WST-1 method), Reduced glutathione (GSH) assay kit, and Malondialdehyde (MDA) assay kit (TBA method) were

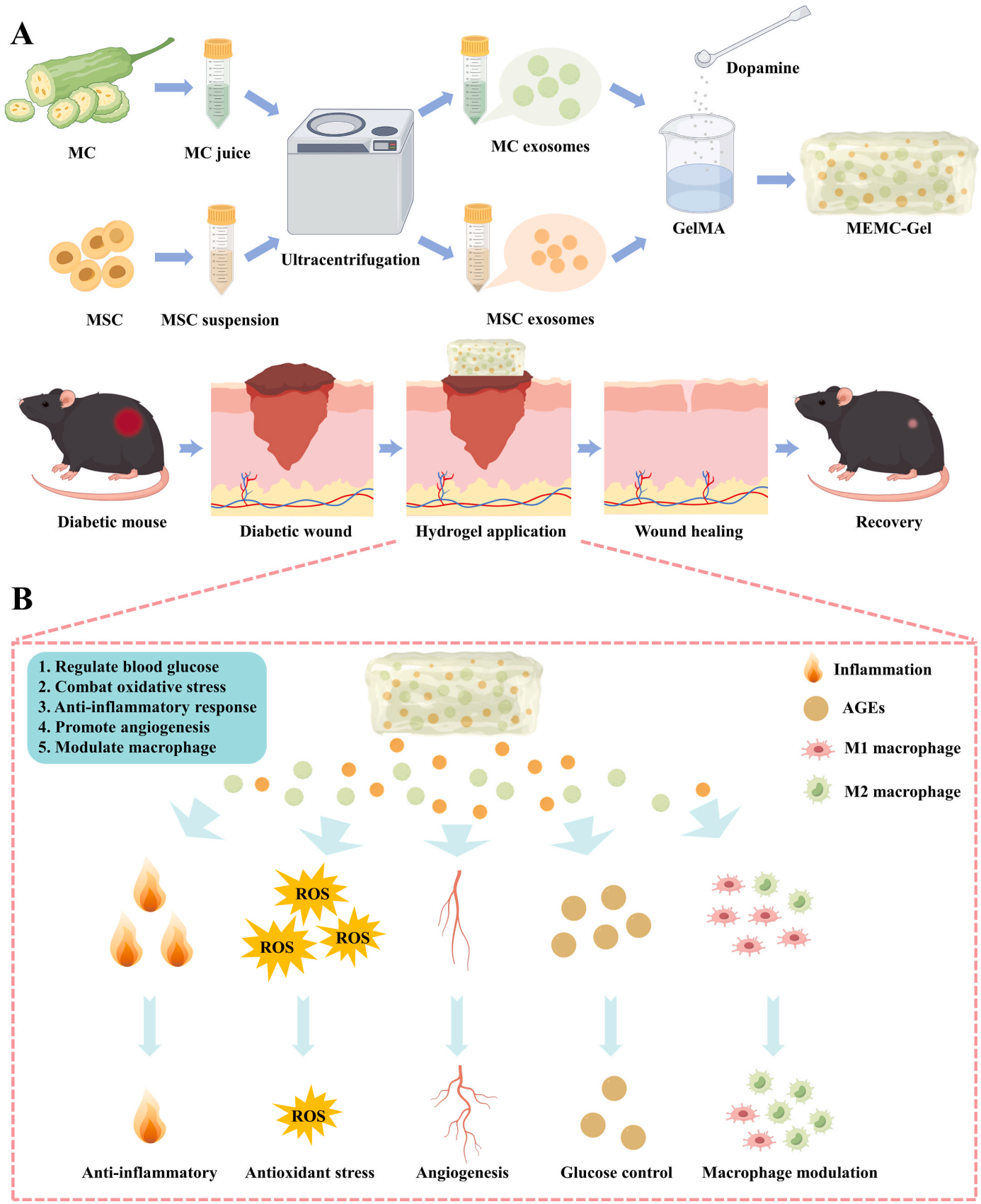

Fig. 1. Schematic diagram of a novel hydrogel loaded with stem cell exosomes and plant exosomes for the treatment of diabetic wounds. (A). Schematic diagram of the synthesis process of MEMC-Gel. (B). Mechanistic process of MEMC-Gel in the treatment of diabetic wounds.

purchased from Nanjing Jiancheng Bioengineering Institute (Nanjing, China). Human umbilical vein endothelial cells (HUVEC) and NIH 3T3 fibroblasts were purchased from Pricella Biotechnology Co., Ltd (Wuhan, China). C57BL/6 mice were obtained from Vital River (Jiaxing, China).

2.2. Isolation of MSC-exo and identification

MSC-exo were isolated by ultracentrifugation [43]. Briefly, the MSC culture supernatant was collected, and dead cells were removed by low-speed centrifugation (2000 g for 10 min). The supernatant was then subjected to successive centrifugation steps: 4 °C, 10,000 g for 30 min; 100,000 g for 60 min; and 100,000 g for 75 min. After each centrifugation, the supernatant was collected, and the pellet was discarded, resulting in the isolation of MSC-derived exosomes (MSC-exo).

The expression of surface markers (CD63, CD9, and CD81) on MSC-exo was assessed by Western blotting. MSC-exos were homogenized using pre-chilled RIPA buffer containing 1 % phosphatase and protease inhibitors. Five times the volume of SDS-PAGE loading buffer was added, and the samples were heated at 100 °C for 10 min to denature the proteins. The proteins were then separated by electrophoresis on a 10 % SDS-PAGE gel and subsequently transferred to a polyvinylidene fluoride (PVDF) membrane via electroblotting. After transfer, the membrane was blocked with 5 % bovine serum albumin (BSA) diluted in PBS at room temperature for 1 h. Following blocking, the membrane was incubated overnight at 4 °C with specific primary antibodies, including CD63 (1:1000), CD9 (1:1000) and CD81 (1:1000). The membrane was then incubated with horseradish peroxidase (HRP)-conjugated secondary antibodies at room temperature for 2 h. Enhanced chemiluminescence (ECL) detection was performed according to the manufacturer's instructions, and the protein bands were visualized using the ChemiDoc™ Touch imaging system (Bio-Rad, California, USA).

2.3. Isolation of MC-exo and identification

MC-exo were isolated according to a modified method based on previous literature [44]. Fresh wild MC was washed three times with tap water, followed by three washes with distilled water, each for approximately 2–3 min. After drying, the MC was cut open, and the seeds were removed, followed by juicing. The extracted MC juice was subjected to successive centrifugation steps: 4 °C, 1000 g for 10 min; 3000 g for 20 min; and 10,000 g for 40 min. After each centrifugation, the supernatant was collected, and the pellet was discarded. The supernatant was then filtered through a 1.0 μm membrane filter and incubated overnight with 8 % PEG8000. The supernatant was subsequently subjected to ultracentrifugation at 4 °C, 150,000 g for 90 min to obtain MC-exo.

As previously reported [45], the RNA enrichment in plant exosomes was assessed to validate MC-exo. Ten microliters of 5 % Triton X-100 were added to the MC-exo, while the control group received an equal volume of PBS. Subsequently, RNA was purified from the resulting mixture using a miRNA isolation kit. The RNA concentration was measured using a Nanodrop (840–317400, Thermo Fisher Scientific, USA).

To further characterize the protein distribution in plant exosomes, MC-exos were homogenized using pre-chilled RIPA buffer containing 1 % phosphatase and protease inhibitors. Five times the volume of SDS-PAGE loading buffer was then added to denature the proteins, followed by incubation at 100 °C for 10 min. The samples were subsequently subjected to electrophoresis on a 10 % SDS-PAGE gel and stained with Coomassie blue. Protein bands were visualized using the ChemiDoc™ Touch imaging system.

2.4. Quantification of exosomes

Twenty microliters of the extracted exosome sample was added to a 96-well plate, and an equivalent volume of BCA working solution (a mixture of BCA reagent A and B diluted at a ratio of 1:50) was added. The contents were gently mixed. The 96-well plate was incubated at 37 °C for 30 min to facilitate the reaction. After incubation, the optical density (OD) was measured at a wavelength of 450 nm using a microplate reader (Varioskan LUX, Thermo Fisher Scientific, USA). The protein concentration in the exosome samples was calculated by comparing the OD values to a standard curve to determine the exosome content.

Each 1×10^6 MSC can yield 59.2 μg of MSC-Exo; each 1 g of MC can yield 6.67 μg of MC-Exo.

The purity of exosomes is calculated using the following formula:

Purity (%) = (RNA concentration after membrane disruption - RNA concentration before membrane disruption)/RNA concentration after membrane disruption.

The purity of MSC-Exo is 73.8 %; the purity of MC-Exo is 53.2 %.

2.5. Exosomes characterization

The morphology of MSC-exo and MC-exo were observed using transmission electron microscopy (TEM) (Hitachi HT7800, Japan). Exosomes were stained with 3 % phosphotungstic acid for 5 min before examination under the TEM. The particle size and zeta potential of the exosomes were measured using a Malvern particle size analyzer (Malvern Zetasizer Nano ZS90, UK). The ultraviolet absorption spectrum of exosomes was obtained using a spectrophotometer (Cary 3500, Agilent Technologies, USA).

2.6. Synthesis of MEMC-Gel

GelMA was synthesized following previously published methods [46]. Concisely, 20 g gelatin was added to 500 mL of pure water. Once the gelatin was dissolved, 20 g $NaHCO_3$ was added. Subsequently, 5 mL of methacrylic anhydride was slowly added while stirring for 1 h. The resulting mixture was placed in a dialysis bag (13,000 Da) and dialyzed at 50 °C for 3 d, with water changes every 3 h. Finally, the dialysate was collected and freeze-dried to obtain GelMA. MEMC-Gel was prepared using the following method: a gel precursor solution was made by dissolving GelMA (10 %, 1 g), DA (2 %, 0.2 g), and LAP (1 %, 0.1 g) in 10 mL PBS before mixing. Exosome solutions (0.5 mL 500 μg/mL MSC-exo and 0.5 mL 500 μg/mL MC-exo) were then added and the mixture was shaken for 1 min. The solution was subsequently exposed to ultraviolet light (wavelength 405 nm) for 40 s to obtain MEMC-Gel. Using a similar method, hydrogels composed solely of GelMA (Gel), hydrogels that do not contain exosomes (B-Gel), hydrogels loaded with MSC-exo (ME-Gel) and hydrogels loaded with MC-exo (MC-Gel) were obtained.

2.7. MEMC-gel characterization

The structural characteristics of MEMC-Gel were observed using scanning electron microscopy (SEM) (ZEISS GeminiSEM 360, Germany). MEMC-Gel was freeze-dried, and the sample was fixed onto the specimen stage. The surface of the sample was then sputter-coated with gold before capturing SEM images. After thorough freeze-drying, the dried product was collected and grounded into a powder. Characterization was performed using fourier transform infrared spectroscopy (FTIR) (Thermo Fisher Scientific Nicolet iS20, USA). Place the hydrogel samples in the sample chamber of the thermogravimetric analyzer (Netzsch TGA 209 F1, Germany) and initiate the instrument to record the curve of mass loss of the samples as a function of temperature. The X-ray diffraction spectra (XRD) of the hydrogel samples were measured using an X-ray diffractometer (Rigaku SmartLab SE, Japan).

2.8. Rheological properties of MEMC-Gel

The rheological behavior of the hydrogels was tested at room temperature using a rheometer (Discovery HR 30, USA) equipped with a 25 mm diameter parallel plate geometry. The storage modulus (G′) and loss

modulus (G″) were recorded to determine the mechanical properties of the hydrogels, while the shear modulus was measured to assess their viscosity.

2.9. Adhesive properties of MEMC-Gel

An electronic universal testing machine (HY 0580, China) was used to evaluate the adhesion capacity of MEMC-Gel. Two pieces of mouse dorsal skin samples were prepared, and adhesive patches were applied with a fixed overlapping area of 10 × 10 mm. The tensile stress was measured at a constant rate of 5 mm/min. The adhesion strength was calculated by dividing the maximum tensile stress by the bonding area to assess the adhesive properties of the hydrogel.

2.10. Degradation experiment

MEMC-Gel was placed in PBS (containing 1 U/mL type II collagenase) and incubated at 37 °C. At predetermined time points, the gel was removed from PBS, freeze-dried, and weighed using a microbalance. The degradation rate was calculated based on the mass loss of the hydrogel.

2.11. Swelling experiment

After freeze-drying, MEMC-Gel was placed in PBS, ensuring that the gel was completely immersed. At predetermined time points, the gel was removed from PBS and weighed using a microbalance. The swelling rate was calculated based on the increase in mass of the hydrogel.

2.12. Exosomes release experiment

A suitable amount of MSC-exo was mixed with 100 μM of the fluorescent dye PKH67. The tube was sealed, vortexed for 1 min, and incubated for 15 min. After incubation, 10 mL of PBS was added to the mixture and thoroughly mixed. Exosomes were then extracted again using the previously described method to remove excess dye, resulting in fluorescently labeled MSC-exo. Similarly, MC-exo were labeled using the PKH26 fluorescent dye following the same procedure. The fluorescently labeled exosomes were then loaded into hydrogels using the aforementioned preparation method. The hydrogel was submerged in PBS (containing 1 U/mL type II collagenase) and incubated at 37 °C. At predetermined time points, 200 μL of the hydrogel eluate was collected, and the fluorescence intensity of both dyes was measured using a microplate reader to assess the release of exosomes.

2.13. Cytotoxicity assay

The cell viability of MEMC-Gel was assessed using the CCK-8 assay in NIH 3T3 cells and HUVEC. Briefly, cells were seeded in 96-well plates at a density of 2.0×10^3 cells per well. In the experimental groups, 20 μL of hydrogel eluate (prepared by submerging the hydrogel in PBS containing 1 U/mL type II collagenase for 8 h, and the subsequent hydrogel eluate were obtained using this method) was added to each well, while the control group received an equivalent volume of PBS. At 1 and 3 days post-treatment, 10 μL of CCK-8 solution was added to each well, and the cells were incubated for 1 h. Absorbance at 450 nm was measured using a microplate reader to evaluate cell viability.

2.14. Cell migration assay

The migratory effect of MEMC-Gel on NIH 3T3 cells was evaluated using the scratch assay to simulate wound healing. NIH 3T3 cells were cultured in 6-well plates until they reached approximately 100 % confluence, and a cell monolayer was scratched using a 200 μL pipette tip. In the experimental groups, 500 μL hydrogel eluate was added to each well, while the control group received an equivalent volume of PBS. Cells were then incubated in serum-free DMEM for 8 and 24 h. Cell migration was captured using a microscope, and the wound width at each time point was analyzed using ImageJ to calculate the migration rate.

2.15. Cell tube formation assay

To evaluate tube formation, 50 μL Matrigel was evenly spread across a 24-well plate and incubated at 37 °C for 30 min. HUVEC were seeded at a density of 1×10^5 cells per well. In the experimental groups, 300 μL hydrogel eluate was added to each well, while the control group received an equivalent volume of PBS. After 8 h of incubation, HUVEC were stained with Calcein-AM, and tube formation was observed using a fluorescence microscope.

2.16. Cellular antioxidant evaluation of MEMC-Gel

NIH 3T3 cells and HUVEC were seeded at a density of 1×10^5 cells per well in 24-well plates. Cells were incubated in serum-free DMEM containing 50 μM DCFH-DA for 30 min, followed by three washes with PBS. Each well was treated with 500 μL of 50 μg/mL ROS inducer (Rosup) for 1 h. In the experimental groups, 300 μL hydrogel eluate was added, while the control group received an equivalent volume of PBS. After 2 h of incubation, cells were washed three times with PBS, and the fluorescence intensity was measured using flow cytometry under dark conditions.

In addition, NIH 3T3 cells and HUVEC were treated in the same manner as described above, but without loading DCFH-DA. The cells were collected into centrifuge tubes using a cell scraper, and 1 mL of PBS was added. The cells were then disrupted using ultrasonic treatment (300 W, ice water bath, sonication for 5 s with intervals, performed 4 times). The samples were centrifuged at 12000 rpm for 15 min at 4 °C to collect the supernatant. Finally, the SOD activity and MDA content were measured using SOD and MDA assay kits to evaluate the intracellular antioxidant capacity of the hydrogels.

2.17. Cellular anti-inflammatory evaluation of MEMC-Gel

RAW 264.7 cells were seeded at 1×10^5 cells per well in 24-well plates and treated with 1 μg/mL LPS for 24 h to induce an inflammatory environment. In the experimental groups, 300 μL hydrogel eluate was added to each well, while the control group received an equivalent volume of PBS. After 12 h of incubation, the concentrations of pro-inflammatory cytokines, including TNF-α, IL-1β, and IL-6, were measured using an enzyme-linked immunosorbent assay (ELISA).

2.18. Assessment of macrophage polarization in MEMC-Gel

Cellular immunofluorescence staining was utilized to assess the polarization status of macrophages [47]. First, Raw 264.7 cells were seeded in a 6-well plate at a density of 2×10^5 cells per well and cultured overnight. The cells were then treated with RPMI 1640 medium containing LPS (1 μg/mL) for 12 h, followed by three washes with PBS. In the experimental group, 600 μL of hydrogel eluate was added for 24h, while the control group received an equal volume of PBS. Next, the old medium was removed, and the cells were washed three times with PBS. The cells were then fixed with 4 % paraformaldehyde at room temperature for 15 min, followed by PBS washes to remove excess fixative. Subsequently, the cells were permeabilized with 0.1 % Triton X-100 for 10 min, and then blocked with 5 % BSA at room temperature for 1 h. After blocking, the cells were incubated overnight at 4 °C with primary antibodies anti-iNOS (1:100) and anti-CD206 (1:50). Following this, fluorescently labeled secondary antibodies were added and incubated at room temperature for 1 h in the dark. DAPI solution was then used to stain the cell nuclei, followed by incubation at room temperature for 5 min and subsequent PBS washes. Finally, the stained cells were observed and imaged using a fluorescence microscope.

2.19. Diabetic animal model

Five-week-old healthy male C57BL/6J mice were selected for the experiment. After one week of acclimatization, the regular diet was replaced with a high-fat diet (60 % of calories from fat), and the mice were continued on this diet for 8 weeks. STZ was prepared freshly by dissolving 10 mg of STZ in 1 mL of 0.1 M citrate-phosphate buffer (pH 4.5) to a final concentration of 1 %. Based on the mice's body weight, STZ was administered intraperitoneally at a dose of 25 mg/kg for 4 consecutive days. Mice were fasted for 12 h before the first injection and provided with food 2 h post-injection. After 4 h, 5 % glucose drinking water was provided, which was switched to normal drinking water after 10 h. For subsequent injections, no fasting was required prior to injection, and the remaining procedures were consistent. One week after the injections, fasting blood glucose levels were measured. Blood glucose levels were measured using a fasting protocol, where mice were fasted from 9 a.m. to 3 p.m. to ensure a 6-h fasting period. Mice with fasting blood glucose levels higher than 16.7 mmol/L were considered successful in the modeling and used for subsequent experiments [48,49]. The successful diabetic mice were randomly divided into five groups: (1) Control group, (2) B-Gel group (blank hydrogel without exosomes), (3) ME-Gel group, (4) MC-Gel group, and (5) MEMC-Gel group, with 8 mice in each group. The mice were anesthetized with an intraperitoneal injection of 3 % pentobarbital sodium (50 mg/kg), followed by hair removal on the dorsal skin using depilatory cream and a hair clipper. A full-thickness 10 mm circular skin wound was created on the dorsal surface of each mouse using a 10 mm skin punch. A 10 mm circular hydrogel dressing was placed on the wound site and secured with an elastic bandage. The day of wound creation was designated as Day 1. Wound healing was assessed by photographing the wounds at Days 1, 3, 7, and 14 post-surgery, and wound area measurements were made using ImageJ software.

2.20. In vivo imaging assessment of MEMC-Gel degradation

Preparation of Cy5-labeled MEMC-Gel for in vivo degradation studies. Specifically, 10 μM of Cy5 dye was mixed into the GelMA solution, and Cy5-labeled MEMC-Gel was prepared using the aforementioned method. The hydrogel was then applied to the surface of diabetic wounds in mice. On days 1, 3, and 7, the fluorescence of MEMC-Gel at the wound was detected using an in vivo imaging system (IVIS Spectrum, PerkinElmer, USA), and the fluorescence intensity was quantitatively analyzed.

2.21. In vivo release of exosomes

PKH67-labeled MSC-exosomes and PKH26-labeled MC-exosomes were loaded into MEMC-Gel using the aforementioned method and then applied to the surface of diabetic wounds in mice. On days 1, 3, and 7, the non-degraded hydrogels were removed from the wound, and then they were placed in 2 mL of 1 U/mL type II collagenase solution in the dark until the hydrogels were completely degraded. A total of 200 μL of the supernatant was collected, and the fluorescence intensity of the two fluorescent dyes was measured using a microplate reader to assess the release of exosomes.

2.22. Histological staining and immunohistochemical analysis

A subset of mice was euthanized, and the wound tissue samples were collected. The tissues were fixed in 4 % paraformaldehyde, followed by routine dehydration, clearing, and embedding in paraffin. Tissue sections were prepared and stained with either H&E or Masson stain. For immunohistochemistry (IHC), deparaffinized and rehydrated sections were subjected to antigen retrieval, followed by blocking of nonspecific binding sites. The sections were then incubated overnight at 4 °C with primary antibodies: anti-MPO (1:100), anti-iNOS (1:100), anti-CD206 (1:100), anti-AEGs (1:100), and anti-CD31 (1:100). After washing, the sections were incubated with the corresponding secondary antibodies at 25 °C for 1 h. Finally, the sections were examined under a light microscope, and images were captured for further analysis.

2.23. DHE fluorescence staining

Wound tissues from the mice were embedded in OCT compound, frozen in liquid nitrogen, and sectioned into 8 μm thick cryosections. The sections were then fixed in 4 % paraformaldehyde at room temperature for 1 h. Under light-protected conditions, the sections were stained with 10 μM DHE for 30 min, followed by DAPI staining for 3 min. Finally, the sections were observed and imaged using a fluorescence microscope.

2.24. Detection of oxidative, inflammatory and angiogenic markers

Wound tissues were collected, washed with ice-cold PBS, and homogenized. The supernatant was then obtained by centrifugation, and the activity of ·OH and SOD, along with the levels of MDA and GSH, were assessed using commercial assay kits according to the manufacturer's instructions. The levels of TNF-α, IL-1β, IL-6, IL-10, TGF-β1 and VEGF in the tissue supernatant were quantified using corresponding ELISA kits, following the manufacturer's protocols. All steps were conducted as per the provided instructions.

2.25. Statistical analysis

The experimental data are presented as the mean ± standard deviation (SD). Differences between groups were assessed using one-way analysis of variance (ANOVA). Statistical significance is denoted as follows: *$p < 0.05$, **$p < 0.01$, ***$p < 0.001$, ****$p < 0.0001$; 'ns' indicates no significant difference. Each experiment was repeated at least three times ($n = 3$).

3. Results and discussion

1 Isolation and characterization of exosomes

First, the supernatant from MSC was collected, and MSC-exo were extracted by ultracentrifugation (Fig. 2A). Similarly, MC-exo were extracted from fresh MC using ultracentrifugation (Fig. 2B). TEM revealed that the MSC-exo had a round vesicular shape (Fig. 2C), and the MC-exo also exhibited a similar round vesicular shape (Fig. 2D), with the MC-exo being slightly larger than the MSC-exo. Further analysis of the exosome size distribution and zeta potential was conducted using a nanoparticle size analyzer (Fig. 2E). The average diameter of MSC-exo was approximately 92.89 nm, and the average diameter of MC-exo was also about 147.20 nm, consistent with the TEM results. The average zeta potential of MSC-exo was approximately -12.50 ± 2.95 mV, while the average zeta potential of MC-exo was about -5.74 ± 3.30 mV (Fig. 2F), indicating similar surface potentials for both types of exosomes. These results suggest that the extracted exosomes are within the typical size range and exhibit characteristic surface charges [50]. It is well known that exosomes contain nucleic acids such as RNA, and UV absorbance spectra recorded an absorption peak at 260 nm, further confirming successful exosome extraction (Fig. S 1A) [51]. Additionally, CD63, CD81, and CD9 are commonly used markers for exosomes derived from stem cells, and these markers are widely employed to confirm the presence and identity of exosomes [52]. Western blot analysis showed significant expression of these exosome markers in the MSC-exo (Fig. 2G), further validating the successful extraction of MSC-exo and providing a reliable basis for subsequent studies. Current research on plant exosomes is still insufficient [53]. Most studies primarily determine the properties of plant exosomes based on TEM morphology and particle size measurements, lacking protein marker analysis [54]. There

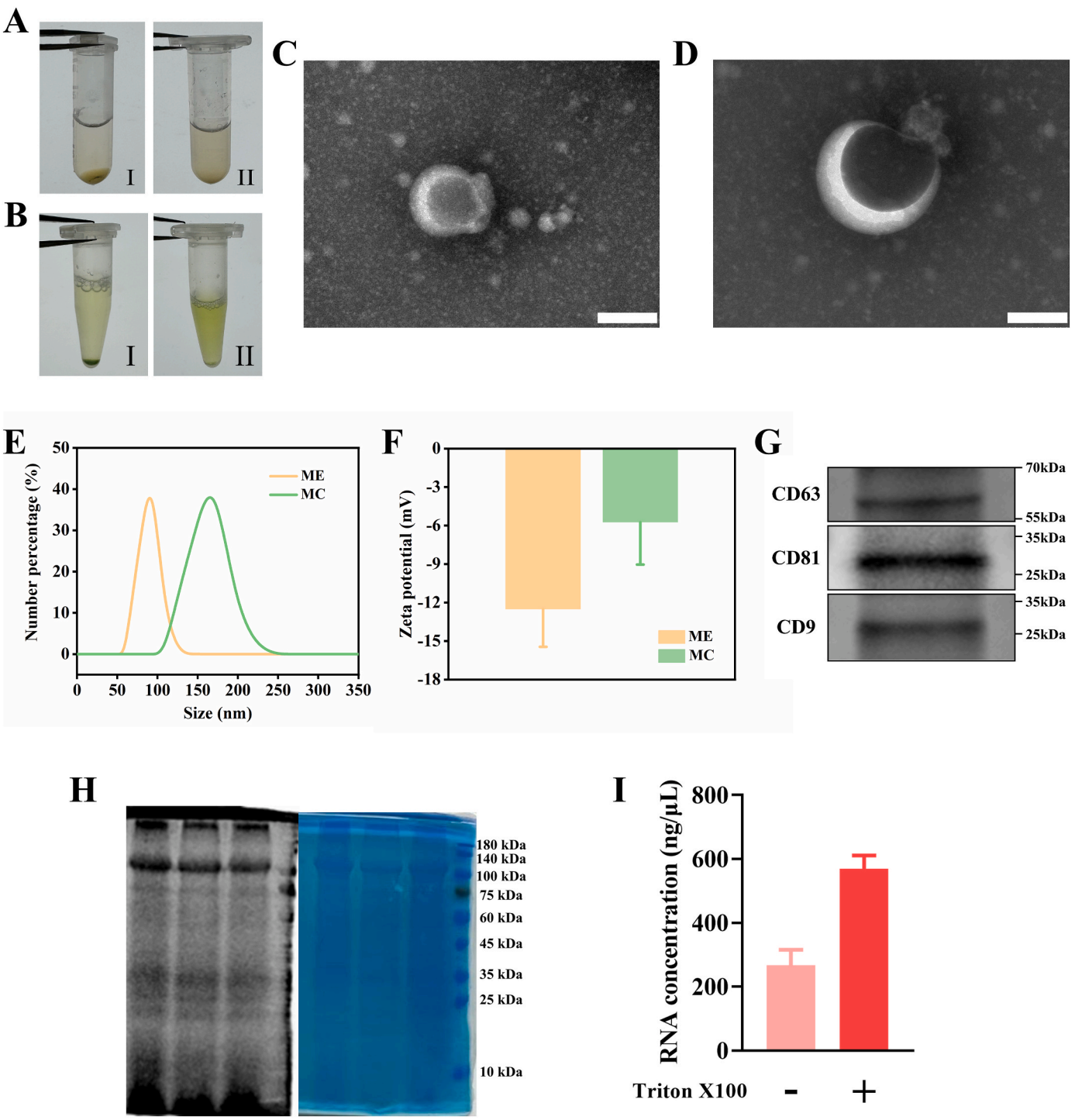

Fig. 2. Exosome characterization. (A). Photograph of MSC-exo. I represents the MSC-exo pellet obtained after ultracentrifugation, with the pellet at the bottom of the EP tube consisting of the extracted MSC-exo. II represents the MSC-exo solution that has been evenly dispersed after pipetting. (B). Photograph of MC-exo. I represents the MC-exo pellet obtained after ultracentrifugation, with the pellet at the bottom of the EP tube consisting of the extracted MSC-exo. II represents the MC-exo solution that has been evenly dispersed after pipetting. (C). TEM reveals the morphology of MSC-exo, with the abundant white material surrounding the MSC-exo representing membrane structures that were disrupted during the exosome extraction process. Scale bar is 100 nm. (D). TEM reveals the morphology of MC-exo, with the abundant white material surrounding the MC-exo representing membrane structures that were disrupted during the exosome extraction process. Scale bar is 100 nm. (E). Size distribution of exosomes. (F). Zeta potential distribution of exosomes (n = 3). (G). Western blot analyses of the MSC-exo surface markers (CD9, CD81, and CD63). (H). Protein gel of MC-exo proteins was prepared. Proteins extracted from MC-exo were separated using 10 % SDS-PAGE and stained with Coomassie blue. (I). The RNA concentration of MC-exo was measured in the presence or absence of Triton X-100 (n = 3). (For interpretation of the references to colour in this figure legend, the reader is referred to the Web version of this article.)

is no consensus on the characteristic markers of plant exosomes. Therefore, based on previous studies [45], we characterized the RNA content and protein distribution in MC-Exo. The molecular sizes of the proteins in MC-ELN were identified through SDS-PAGE (Fig. 2H), indicating that the protein distribution of MC-Exo mainly falls within the range of 10–140 kD. Next, by measuring the RNA content of MC-Exos before and after the addition of Triton X-100, we confirmed that the extracted MC-Exos contain a substantial amount of RNA, which is a characteristic marker of exosomes (Fig. 2I).

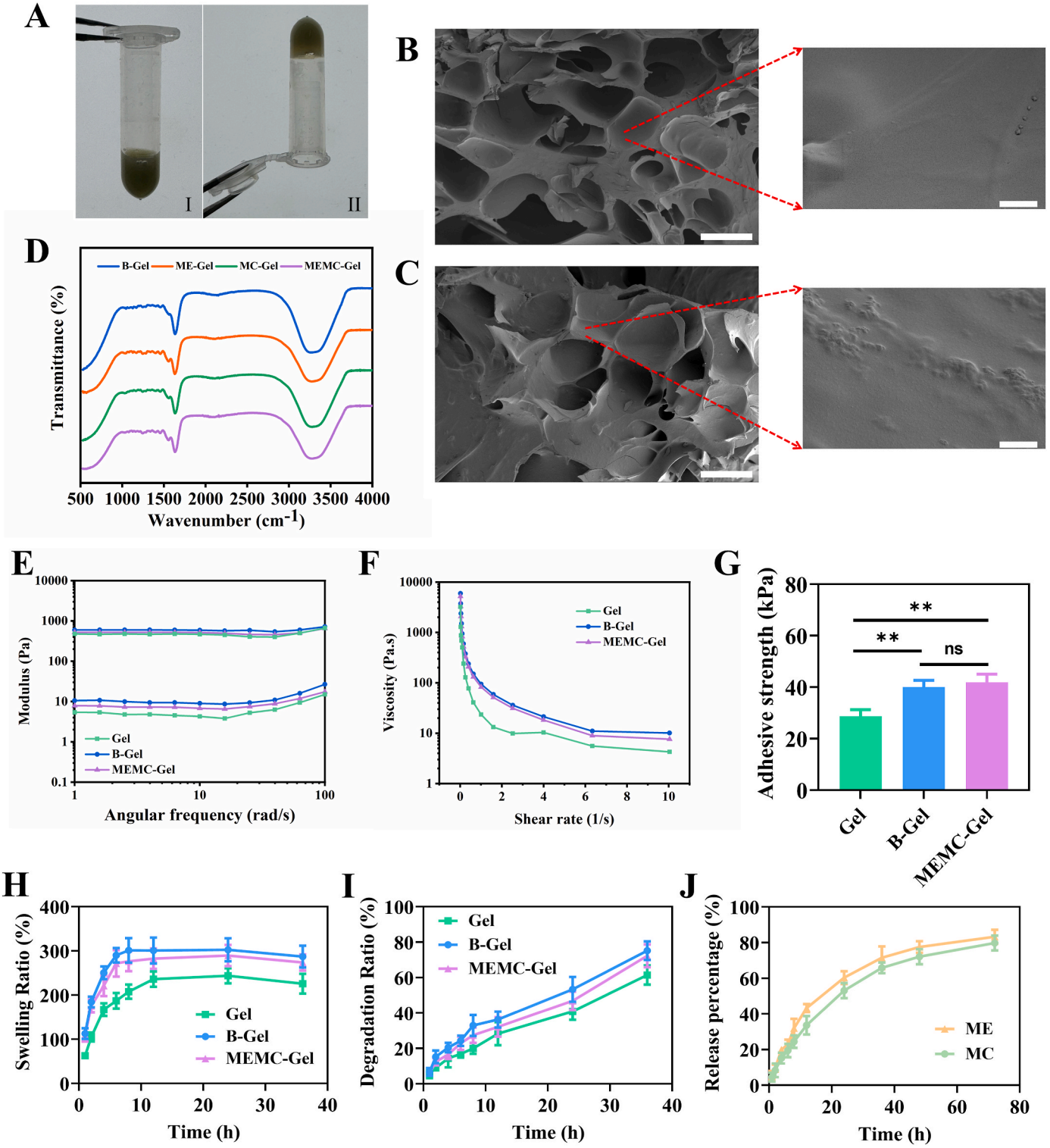

Fig. 3. MEMC-Gel characterization. (A). Physical appearance of the hydrogel before (I) and after gelation (II). (B). TEM image of B-Gel. Scale bar: upper is 100 μm; lower is 20 μm. (C). TEM image of MEMC-Gel. Scale bar: upper is 100 μm; lower is 20 μm. (D). FTIR spectra of B-Gel, ME-Gel, MC-Gel and MEMC-Gel. (E). Storage (G′) and loss (G″) modulus of Gel, B-Gel and MEMC-Gel. (F). Shear viscosity of Gel, B-Gel and MEMC-Gel. (G). Viscosity of Gel, B-Gel and MEMC-Gel (n = 3). (H). Swelling ratio of Gel, B-Gel and MEMC-Gel in PBS at different time scales (n = 3). (I). Degradation ratio of the Gel, B-Gel and MEMC-Gel in PBS at different time scales (n = 3). (J). Release percentage curve of MSC-exo and MC-exo in MEMC-Gel (n = 3).

2 Preparation and characterization of MEMC-Gel

The methacrylamide groups were grafted onto gelatin through a free radical polymerization reaction to obtain GelMA, which has ultraviolet (UV) crosslinking capabilities. Gel was dissolved in PBS and mixed with dopamine (DA) and two types of exosomes (Fig. 3A). UV light exposure then facilitated the crosslinking of Gel and DA, forming a stable hydrogel structure. The incorporation of DA not only enhances the mechanical strength and surface adhesion of the hydrogel but also improves its stability and biocompatibility through its self-polymerizing properties [55]. Exosomes, on the other hand, are stably encapsulated in the hydrogel matrix and are gradually released as the hydrogel degrades, exerting their therapeutic effects [42]. First, the microscopic structure of B-Gel (Blank hydrogel without exosomes) and MEMC-Gel was observed using scanning electron microscopy (SEM). B-Gel exhibited a relatively typical porous network structure with uniformly distributed pores and a regular morphology (Fig. 3B). In the microstructure of MEMC-Gel, exosomes were evenly dispersed throughout the hydrogel (Fig. 3C). FTIR spectroscopy was used to analyze B-Gel ME-Gel, MC-Gel and MEMC-Gel (Fig. 3D). The infrared spectra of the four groups showed significant overlap, with no obvious differences in the major peaks. Analysis of the infrared absorption characteristic peaks indicated that there were no significant differences in the types and quantities of internal functional groups among the four samples. This suggests that the incorporation of exosomes into the hydrogel is a physical interaction, and no chemical reactions occurred between the exosomes and the hydrogel components. Additionally, we characterized each group using X-ray diffraction and found that the peaks of the four curves almost coincided, indicating that the presence of exogenous materials did not affect the internal structure of the hydrogel (Fig. S 1B). Thermogravimetric analysis (TGA) showed that MEMC-Gel maintained good thermal stability (Fig. S 1C), with rapid mass loss occurring only when the temperature exceeded 260 °C, suggesting that MEMC-Gel has excellent thermal stability under normal conditions.

Next, the rheological properties of MEMC-Gel were measured. The results revealed that MEMC-Gel exhibited a slightly higher storage modulus (G′) than loss modulus (G″), indicating good mechanical properties (Fig. 3E). Gel (formed solely by GelMA), serving as the base material for the hydrogel, exhibits typical hydrogel behavior. When DA is incorporated to form B-Gel, although there is an improvement in mechanical properties, the change is not significant. After the inclusion of exosomes in MEMC-Gel, it still maintains mechanical properties similar to those of B-Gel. This indicates that the addition of exosomes does not have a negative impact on the mechanical stability of the gel. MEMC-Gel displayed shear thinning behavior (Fig. 3F), which facilitated easier application to the target site during the coating process and ensured uniform distribution [56]. This property is particularly advantageous in applications such as wound dressings, drug delivery systems, or skin patches, where it can effectively conform to various shapes and surface conditions. Importantly, the introduction of exosomes did not alter the rheological properties of the hydrogel. To further evaluate the adhesive properties of MEMC-Gel, it was sandwiched between two pieces of mouse dorsal skin, and its viscosity was measured to be 41.87 ± 3.15 kPa, showing no significant difference compared to B-Gel (Fig. 3G). This further demonstrates that the incorporation of exosomes does not affect the adhesive properties of MEMC-Gel. Notably, the adhesive strength of Gel was significantly lower than that of B-Gel and MEMC-Gel, which indicates that the introduction of DA significantly enhances the adhesive properties of the hydrogel. Additionally, the swelling ability of MEMC-Gel was assessed. Compared to Gel, both B-Gel and MEMC-Gel rapidly absorbed water in PBS and reached near equilibrium within 10 h (Fig. 3H). This indicates that the addition of DA increases the hydrophilicity of MEMC-Gel and also shows that MEMC-Gel can absorb water quickly and maintain notable stability. To further clarify the influence of DA on the hydrophilicity of hydrogels, the hydrophilic performance of the hydrogel was evaluated by measuring the contact angle of water droplets just when they came into contact with the hydrogel surface. A smaller contact angle indicates better hydrophilicity of the hydrogel. The results showed that Gel had a relatively large contact angle, suggesting poor hydrophilicity. In contrast, the contact angles of B-Gel and MEMC-Gel were significantly reduced (Fig. S 2A and B), which directly demonstrated that dopamine can effectively enhance the hydrophilicity of hydrogels. This indicates that MEMC - Gel can interact more effectively with wound exudate. This makes them highly effective in managing wound exudates, exhibiting superior water absorption and regulation. Degradation studies of MEMC-Gel showed that the hydrogel degraded by more than 50 % within 24 h (Fig. 3I), ensuring that exosomes were gradually released as the hydrogel degraded, thus meeting the demand for exosome delivery during wound healing. These experimental results collectively suggest that MEMC-Gel has excellent potential for use in wound dressings and drug delivery systems in biomedical applications. Finally, the exosome release capability of MEMC-Gel was determined by staining both MSC-exo and MC-exo, followed by measuring the fluorescence intensity in the supernatant of the hydrogel (Fig. 3J). The results demonstrated that MEMC-Gel could effectively control the release of exosomes, with no significant difference in the release rates of the two types of exosomes, further confirming that MEMC-Gel holds significant advantages for sustained exosome delivery applications. However, we must consider that while collagenase was used in the degradation and release experiments to simulate in vivo degradation, a single type of collagenase cannot adequately replicate the complex environment of a wound. There are inherent differences between the degradation kinetics of the hydrogel in vivo and in vitro, which necessitate further research. Additionally, the observed release of exosomes may be attributed to the diffusion of the fluorescent dye through the exosomal membrane prior to the enzymatic degradation of the hydrogel. To better confirm the release of exosomes, we conducted further experiments to validate the exosome release both in vivo and in vitro.

On the other hand, in the subsequent in vitro experiments, the eluate of MEMC-Gel was used for further studies. It is of great necessity to identify the active components in the MEMC-Gel eluate. For this purpose, we collected the 8 h eluate of MEMC-Gel and observed its components via TEM. The results revealed that the leachate contained a large quantity of exosomes and degraded exosome fragments (***Fig. S 3A***). The infrared spectrum analysis of the eluate reveals a broad absorption peak in the range of 3400–3500 cm^{-1}, which is primarily attributed to the stretching vibrations of amino and hydroxyl groups. This indicates a significant presence of hydrogen-bonded compounds in the MEMC-Gel leachate, likely stemming from the hydroxyl and amino groups in DA molecules. Additionally, the absorption peaks in the range of 1650–1700 cm^{-1} are mainly associated with C=O stretching vibrations, suggesting the presence of amide (C=O) chemical structures in the eluate, which is consistent with the amide groups within the GelMA molecular backbone (Fig. S 3B). These findings collectively confirm through FTIR analysis that the eluate contains DA, GelMA, and their degradation products. Identifying the active components in the MEMC-Gel eluate will provide a clearer and more precise foundation for subsequent in - depth research on its therapeutic mechanisms and efficacy.

3 In vitro cell studies of MEMC-Gel

We first assessed the cytotoxicity of MEMC-Gel using the CCK-8 assay. To evaluate the biocompatibility of MEMC-Gel, we selected NIH 3T3 fibroblasts and HUVEC as in vitro models, as these cell types are commonly used to study human skin cell behavior and function and have been widely applied in relevant literature [57]. Testing with these cell models effectively evaluated the biocompatibility of MEMC-Gel. The CCK-8 results demonstrated that MEMC-Gel did not exhibit significant cytotoxicity to either NIH 3T3 cells or HUVEC, indicating its good cellular compatibility and suitability as a biomaterial for medical applications (Fig. 4A and B). A scratch assay, a commonly used method to

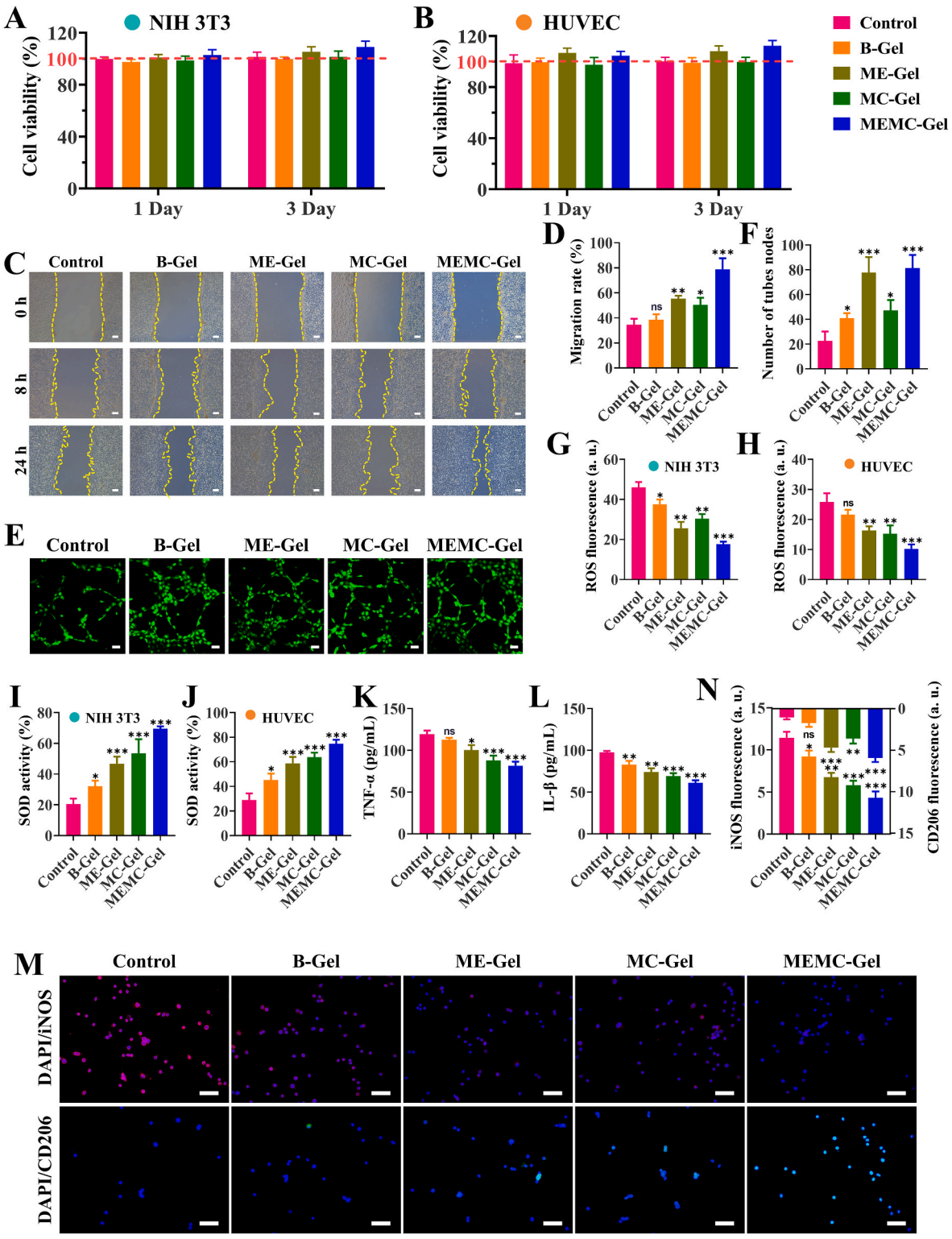

Fig. 4. In vitro properties and safety of MEMC-Gel. (A). Cell viability of NIH 3T3 cells treated with hydrogel. (B). Cell viability of HUVEC treated with hydrogel. (C). Cell scratch assay of NIH 3T3 cells treated with hydrogel. Scale bar is 100 μm. (D). Cell migration rate of NIH 3T3 cells treated with hydrogel (n = 3). (E). Tube formation assay of HUVEC treated with hydrogel. Scale bar is 50 μm. (F). Quantitative analysis of tube formation in the tube formation assay (n = 3). After treatment with ROS-positive inducing drugs and hydrogels, the ROS levels in NIH 3T3 cells (G) and HUVEC (H) were assessed using flow cytometry, followed by quantitative analysis of the flow cytometry results (n = 3). Detection of SOD concentration in NIH 3T3 cells (I) and HUVEC (J) after treatment with ROS-positive inducing drugs and hydrogels (n = 5). After LPS stimulation and hydrogel treatment, the levels of (K) TNF-α and (L) IL-1β in RAW 264.7 cells were measured using ELISA (n = 5). (M). Cellular immunofluorescence of the polarization status of Raw 264.7 cells treated with hydrogel. Scale bar is 100 μm. (N). Quantitative analysis of the immunofluorescence intensity of iNOS and CD206 (n = 3). All data are shown as the mean ± SD. Compared with control group, ns ≥ 0.05, *p < 0.05, **p < 0.01, ***p < 0.001.

assess cell migration and interactions, was conducted to simulate cell migration during wound healing and to evaluate the effects of the hydrogel on cells [58]. In this study, we used the scratch assay to evaluate the effect of MEMC-Gel on NIH 3T3 cell migration. The results showed that MEMC-Gel significantly promoted cell migration (Fig. 4C), especially after 24 h of treatment, when the migration rate and healing ability were notably enhanced, with migration rate reaching 78.87 ± 8.75 % (Fig. 4D). Furthermore, MSC-exo exhibited superior cell migration-promoting effects compared to MC-exo. The combined use of both exosomes further enhanced the migration-promoting effect. This finding further validated that MEMC-Gel effectively promotes wound healing in vitro. These results suggest that MEMC-Gel accelerates cell migration, a crucial process for wound closure and tissue regeneration. The tube formation assay, a method used to evaluate endothelial cell ability to form vessel-like structures on matrix materials [59], was performed to assess the angiogenic effects of MEMC-Gel. The results revealed that MEMC-Gel significantly promoted tube formation by HUVEC on the hydrogel surface, where cells rapidly aggregated and formed tubular structures (Fig. 4E), with the number of tubes reaching 81.33 ± 10.59 (Fig. 4F). In addition, B-Gel also exhibited some degree of angiogenic effect on HUVEC. However, MSC-exo exhibited far greater pro-angiogenic effects than MC-exo, suggesting that the angiogenic effect of MEMC-Gel is primarily attributed to the action of MSC-exo. In summary, MEMC-Gel not only supports cell growth and migration but also effectively promotes angiogenesis, enhancing its potential in tissue repair and regeneration, particularly in promoting wound healing and improving local blood supply.

Subsequent, to further investigate the antioxidant capacity of MEMC-Gel, NIH 3T3 cells and HUVEC were loaded with DCFH-DA, and an oxidative stress environment was induced by adding Rosup (ROS inducer). After co-culturing the cells with hydrogel eluate for a period of time, the fluorescence intensity in the cells was measured by flow cytometry (Fig. S 4A and B). DCFH-DA enters cells and is hydrolyzed by esterases to DCFH. The ROS inside the cells oxidize the non-fluorescent DCFH to fluorescent DCF, and changes in fluorescence intensity reflect the level of ROS in the cells. Flow cytometry results showed that the fluorescence intensity in the MEMC-Gel group was significantly lower than in the control group. Both ME-Gel and MC-Gel groups exhibited similar fluorescence intensity, also lower than the control group (Fig. 4G and H), indicating that MEMC-Gel can effectively reduce intracellular ROS levels, thereby alleviating oxidative stress. The antioxidant effects of MSC-exo and MC-exo in vitro were similar, and their combined action further enhanced the antioxidant effect. On the other hand, the pure hydrogel also demonstrated some antioxidant properties. Superoxide dismutase (SOD) is a crucial antioxidant enzyme that catalyzes the dismutation of superoxide anions into hydrogen peroxide and oxygen, thereby mitigating oxidative damage. Malondialdehyde (MDA) is a product of lipid peroxidation, and its level reflects the extent of oxidative damage to cell membrane lipids. To further validate the antioxidant capacity of MEMC-Gel, we measured the activity of SOD and the level of

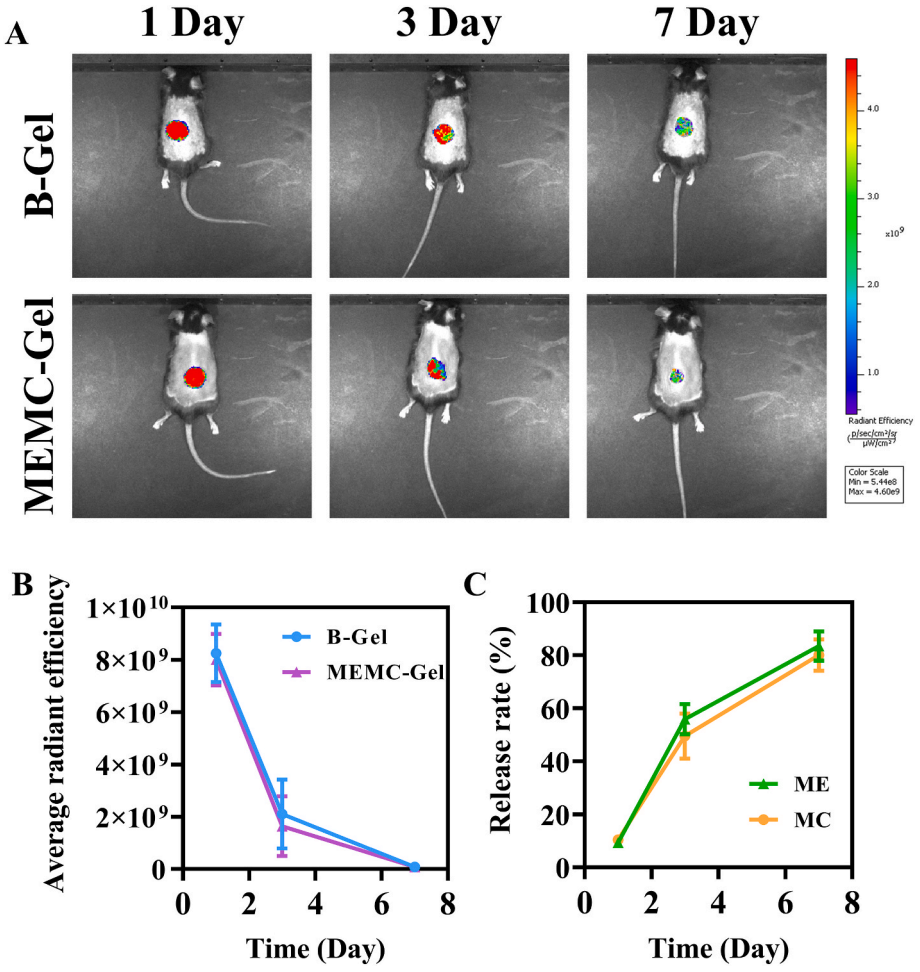

Fig. 5. In vivo degradation and release of MEMC-Gel. (A). In vivo imaging of the degradation of Cy5-labeled B-Gel and MEMC-Gel at the wound on days 1, 3, and 7 post-application. (B). Fluorescence quantitative analysis of in vivo imaging (n = 3). (C). In vivo release of PKH67-labeled MSC-exosomes and PKH26-labeled MC-exosomes at the wound on days 1, 3, and 7 post-application (n = 3). All data are shown as the mean ± SD. Compared with control group, ns ≥ 0.05, *p < 0.05, **p < 0.01, ***p < 0.001.

MDA in NIH 3T3 cells and HUVEC under oxidative stress stimulation. The experimental results demonstrated that, compared to the control group, the MEMC-Gel treatment group exhibited a significant increase in SOD activity and a significant reduction in MDA levels (Fig. 4I and J; Fig. S 5A and B). The ME-Gel and MC-Gel treatment groups also showed similar antioxidant effects, although their efficacy was relatively weaker compared to MEMC-Gel. This indicates that the synergistic action of MSC-exo and MC-exo in MEMC-Gel significantly enhances its antioxidant capacity. These findings suggest that MEMC-Gel not only mitigates oxidative damage to cells by enhancing SOD activity but also reduces MDA levels, thereby alleviating lipid peroxidation-induced damage to cell membranes. Furthermore, 2,2′-azino-bis(3-ethylbenzothiazoline-6-sulfonic acid) (ABTS) is a widely used method to assess the free radical scavenging ability of antioxidants. The ability of a substance to inhibit the oxidation of ABTS to form radical cations reflects its antioxidant potential. Therefore, we also carried out an ABTS radical inhibition assay on the hydrogel. The experimental results showed that the MEMC-Gel group had the highest inhibition rate of ABTS, further confirming its excellent antioxidant activity (Fig. S 5C). Notably, the B-Gel also exhibited a moderate ability to inhibit ABTS, indicating that the hydrogel itself also possesses certain antioxidant capacity. In conclusion, these findings underscore the remarkable antioxidant efficacy of MEMC-Gel, which not only reduces ROS accumulation and combats oxidative stress by enhancing cellular defense mechanisms but also provides a protective barrier against lipid peroxidation, minimizing cellular damage. This provides a robust theoretical basis for its potential application in the treatment of oxidative stress-related diseases and tissue repair.

RAW 264.7 cells, a common mouse macrophage cell line widely used to study inflammatory responses, were stimulated with lipopolysaccharide (LPS) to simulate cellular inflammation [60]. After stimulation, hydrogel eluate was added, and at the designated time points, the levels of inflammatory cytokines (TNF-α, IL-1β, and IL-6) in the culture supernatant were measured using ELISA. In the LPS-stimulated control group, the levels of TNF-α and IL-1β were significantly elevated, confirming the successful activation of the inflammatory response. Compared to the control group, the MEMC-Gel group showed a significant reduction in TNF-α and IL-1β levels, with decreases of 37.85 ± 1.87 pg/mL and 36.40 ± 3.71 pg/mL (Fig. 4K and L), respectively, indicating that MEMC-Gel effectively inhibited LPS-induced inflammation and exhibited strong anti-inflammatory effects. Similarly, the level of IL-6 was also significantly reduced in the MEMC-Gel group, with a decrease of 31.71 ± 3.82 pg/mL (Fig. S 5D), further confirming its effectiveness in suppressing inflammatory cytokines. These results highlight the potent anti-inflammatory properties of MEMC-Gel, suggesting its potential to modulate the inflammatory response in pathological conditions. By effectively reducing key inflammatory cytokines such as TNF-α, IL-1β, and IL-6, MEMC-Gel may help to limit the detrimental effects of excessive inflammation, which is often observed in chronic wounds and inflammation-related diseases. The ability of MEMC-Gel to inhibit inflammation makes it a promising candidate for therapeutic interventions targeting both acute and chronic inflammatory conditions, particularly in wound healing and chronic inflammation treatment.

As important immune cells, the polarization states of macrophages play a crucial role in maintaining the immune microenvironment of wounds and promoting wound healing. Therefore, we further investigated the in vitro effect of MEMC - Gel on macrophage polarization. LPS was used to mimic the inflammatory environment of diabetic wounds, and RAW 264.7 cells were stimulated with hydrogel eluate for 24 h. The polarization status of RAW 264.7 cells was determined by immunofluorescence staining of inducible nitric oxide synthase (iNOS, a characteristic protein of M1 macrophages) and CD206 (a characteristic protein of M2 macrophages). Compared with the control group, after the RAW 264.7 cells were stimulated with the leaching solutions of ME-Gel, MC-Gel, and MEMC-Gel, the fluorescence level of iNOS decreased, while the fluorescence level of CD206 increased (Fig. 4M). Quantitative analysis of the immunofluorescence data further confirmed these observations. The control group exhibited the highest iNOS fluorescence intensity, whereas the MEMC-Gel group showed the highest CD206 fluorescence intensity (Fig. 4N). These results suggest that MEMC-Gel significantly promotes the polarization of macrophages towards the M2 phenotype, which is associated with anti-inflammatory and tissue-repair functions, while simultaneously suppressing the M1 phenotype, which is linked to pro-inflammatory responses. The ability of MEMC-Gel to modulate macrophage polarization highlights its potential as a therapeutic agent for enhancing wound healing, particularly in the context of diabetic wounds where chronic inflammation and impaired healing are prevalent.

4 MEMC-Gel degradation and exosome release in vivo

To further investigate the degradation of MEMC-Gel in vivo, a full-thickness wound model was established on the backs of diabetic mice. Cy5-labeled MEMC-Gel was used to study the degradation process. Cy5-labeled MEMC-Gel and Cy5-labeled B-Gel were applied to the wounds on the mice. Fluorescence signals from MEMC-Gel were detected using an in vivo imaging system on days 1, 3, and 7. It was observed that by day 7, the fluorescence intensity of the hydrogels significantly decreased (Fig. 5A). Quantitative analysis further confirmed that the majority of MEMC-Gel had degraded by day 7 in vivo, similar to B-Gel (Fig. 5B). This suggests that the incorporation of exosomes does not significantly affect the degradation capacity of the hydrogel. PKH67-labeled MSC-exosomes and PKH26-labeled MC-exosomes were applied to the wounds of diabetic mice to investigate the release profiles of exosomes in vivo. As the hydrogels degraded, both types of exosomes were gradually released at similar rates, with over 50 % of the exosomes being released within the first three days (Fig. 5C). The experimental results indicate that MEMC-Gel, as a drug delivery system, exhibits favorable degradation and exosome release characteristics in vivo.

5 MEMC-Gel promotes wound healing in diabetic mice

To comprehensively evaluate the potential of MEMC-Gel in promoting diabetic wound healing in vivo, we conducted an in vivo experiment using a diabetic mouse model with full-thickness skin defects (Fig. 6A). The mice were first subjected to an 8-week high-fat diet followed by intraperitoneal injection of STZ. Upon confirming the successful establishment of the diabetic model, a 10 mm diameter wound was created on the back of the diabetic mice using a skin puncher, referred to as the diabetic wound. MEMC-Gel was then applied to the wound surface, and its therapeutic effect was compared with the control group. The remaining wound area for each wound was recorded and measured on days 1, 3, 7, and 14 (Fig. 6B). Before day 7, both the ME-Gel and MC-Gel groups exhibited similar healing trends, indicating that both MSC-exo and MC-exo positively affected wound healing and could promote wound closure in the short term. On day 14, the wound healing rate in the ME-Gel group slightly surpassed that of the MC-Gel group, suggesting that MSC-exo might have greater potential in accelerating wound healing. However, only the MEMC-Gel group experienced the most accelerated wound healing process, with the wound healing rate reaching 78.14 ± 4.02 % on day 7 and achieving near-complete closure by day 14 (Fig. 6C and D). These findings suggest that while ME-Gel or MC-Gel groups alone show some early (before day 7) wound healing promotion, their long-term (day 14) efficacy does not match that of the MEMC-Gel group. This indicates that while MSC-exo or MC-exo alone can improve wound healing in the short term, there is still room for improvement in their therapeutic effects. In contrast, the MEMC-Gel, which contains both exosomes, significantly enhances the overall wound healing outcome. These results demonstrate the clear advantages of MEMC-Gel in promoting wound healing and tissue regeneration.

To further validate the therapeutic effects of MEMC-Gel, histological analyses using H&E staining and Masson staining were performed to

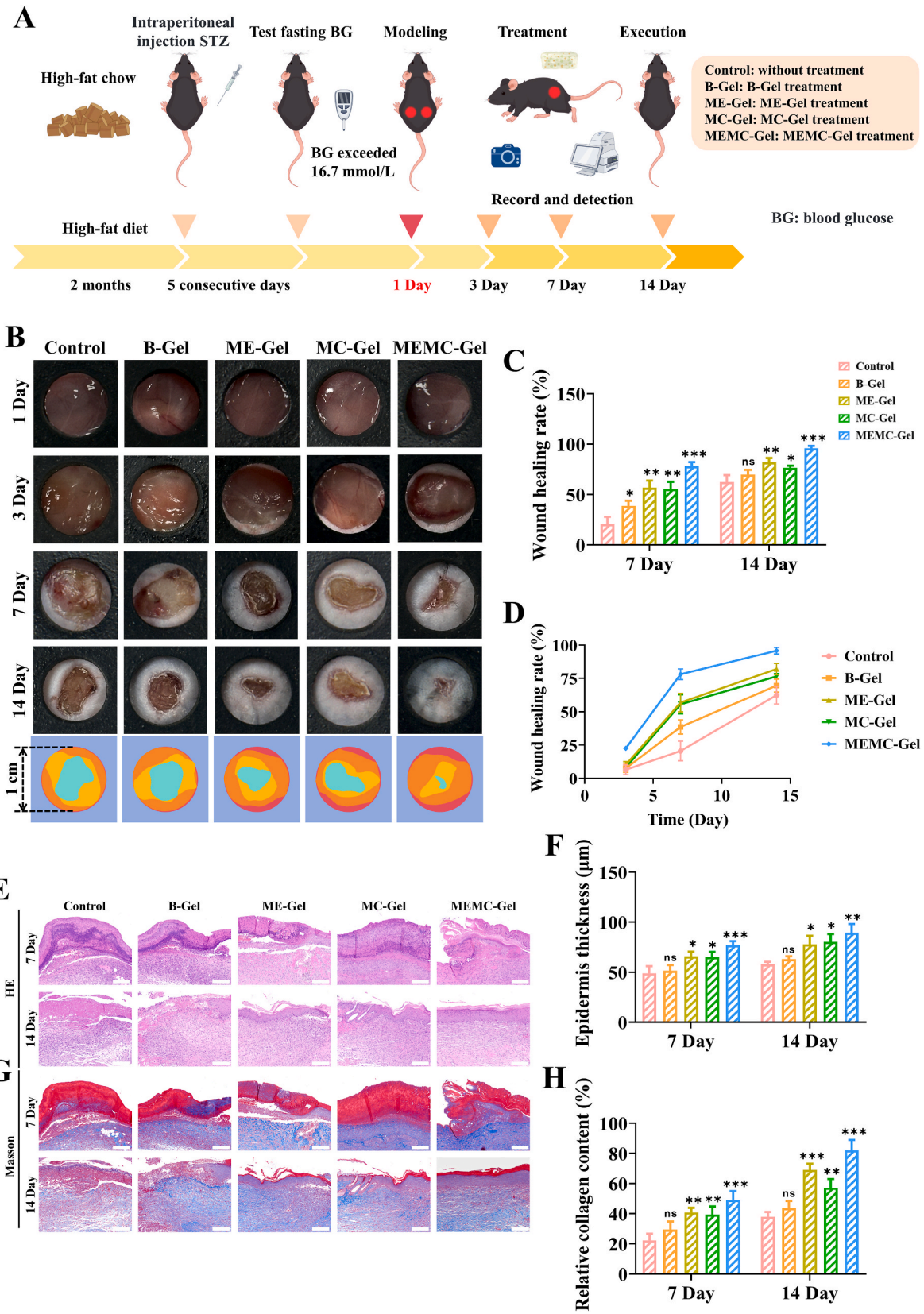

Fig. 6. MEMC-Gel enhances the healing of diabetic wounds. (A). Timeline illustration of animal experiments using MEMC-Gel for the treatment of diabetic wounds. (B). Representative photographs of wound healing at different time points after various treatments. (C). Wound healing rates at different time points after various treatments (n = 3). (D). Wound healing rates over time following different treatments (n = 3). (E). H&E staining of wound tissue at different time points following various treatments. Scale bar is 200 μm. (F). Quantitative analysis of thickness of the epidermis of wound tissue (n = 3). (G). Masson staining of wound tissue at different time points following various treatments. Scale bar is 200 μm. (H). Quantitative analysis of collagen deposition of wound tissue (n = 3). All data are shown as the mean ± SD. Compared with control group, ns ≥ 0.05, *p < 0.05, **p < 0.01, ***p < 0.001.

observe the tissue structure of the wounds. H&E staining showed significant inflammatory cell infiltration in the early healing phase (day 7). The MEMC-Gel group exhibited the least inflammatory cell infiltration, followed by the ME-Gel and MC-Gel groups. By day 14, inflammatory cell infiltration further decreased in all groups. As healing progressed, the MEMC-Gel group showed epithelial regeneration, the formation of mature new blood vessel networks, and normal skin tissue structure, indicating good wound healing (Fig. 6E). On day 14, the ME-Gel and MC-Gel groups showed an increase in epidermal thickness compared to the control group, with the MEMC-Gel group displaying the most significant increase in epidermal thickness, highlighting its superior ability to promote epidermal regeneration and repair (Fig. 6F). Furthermore, Masson staining revealed a significant increase and remodeling of collagen fibers in the MEMC-Gel group (Fig. 6G), from 49.16 ± 5.79 % on day 7–82.14 ± 6.79 % on day 14 (Fig. 6H). In contrast, although the collagen fiber increase in the ME-Gel and MC-Gel groups was notable, it did not match the extent of the MEMC-Gel group. Besides, over time, the ME-Gel group showed a better increase in collagen fibers than the MC-Gel group, indicating that MSC-exo have a stronger efficacy in promoting collagen fiber deposition and tissue remodeling. The enhanced collagen deposition and remodeling in the MEMC-Gel group suggest its potential in promoting stronger and more resilient tissue repair. Overall, compared to control group, the MEMC-Gel, ME-Gel, and MC-Gel experimental groups all displayed significant reductions in inflammatory response, increased granulation tissue, epithelial cell regeneration, and improved collagen fiber deposition. However, the MEMC-Gel stood out in these aspects, further proving its superiority in promoting diabetic wound healing.

6 Anti-inflammatory effects of MEMC-Gel in diabetic wounds

Inflammation is a major factor that hinders wound healing. To further investigate the anti-inflammatory effect of MEMC-Gel in diabetic wounds, we first performed MPO immunohistochemical (IHC) staining on the wound tissues of the mice. MPO is a marker of neutrophil infiltration, and its expression level is closely related to the intensity of the inflammatory response [61]. On day 7, compared to the control group, the MEMC-Gel group exhibited a significant reduction in MPO-positive cells, indicating a marked decrease in neutrophil infiltration. Both the ME-Gel and MC-Gel groups showed fewer MPO-positive cells than the control group, with the MC-Gel group having a slightly lower MPO-positive expression rate than the ME-Gel group. This suggests that

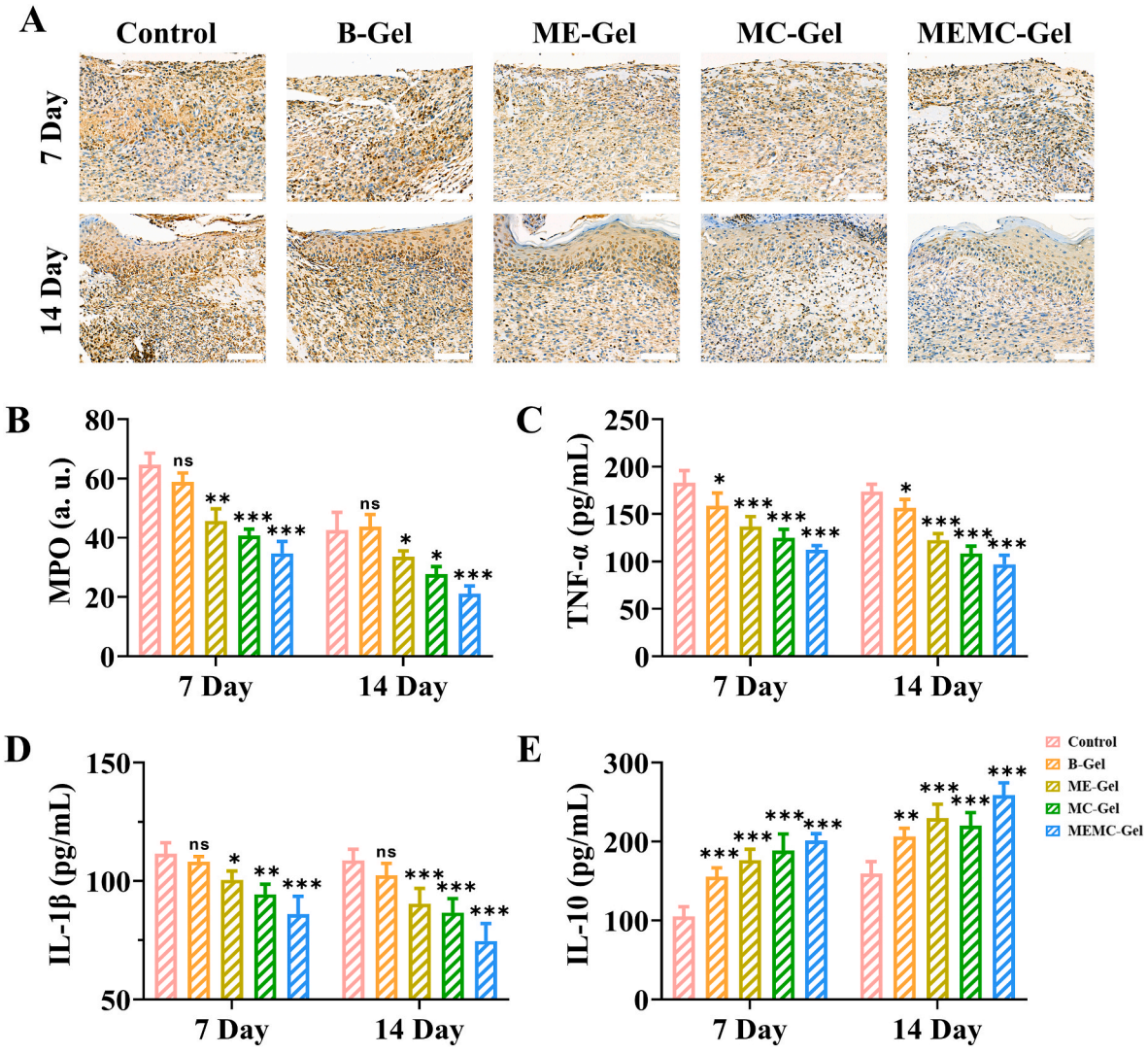

Fig. 7. Anti-inflammatory effects of MEMC-Gel in animal experiments. (A). IHC staining of MPO of wound tissue at different time points following various treatments. Scale bar is 100 μm. (B). Quantitative analysis of MPO expression of wound tissue (n = 3). The levels of inflammatory cytokines in wound tissue at different time points following various treatments: (C) TNF-α, (D) IL-1β and (E) IL-10 (n = 5). All data are shown as the mean ± SD. Compared with control group, ns ≥ 0.05, *p < 0.05, **p < 0.01, ***p < 0.001.

the MC-Gel group has a slightly superior anti-inflammatory effect compared to the ME-Gel group, although still less pronounced than that of MEMC-Gel. By day 14, the number of MPO-positive cells had further decreased in all groups, but the MEMC-Gel group still displayed the lowest MPO-positive levels (Fig. 7A and B), indicating that MEMC-Gel effectively suppresses neutrophil infiltration, thereby alleviating local inflammation. The significant reduction in MPO-positive cells, particularly in the MEMC-Gel group, highlights its potent anti-inflammatory properties, which are crucial for accelerating wound healing in diabetic wounds where excessive inflammation can delay recovery.

To further validate the anti-inflammatory effects of MEMC-Gel, we measured the levels of key inflammatory cytokines (TNF-α, IL-1β, and IL-6) in the wound tissues of the mice using ELISA. The results showed that on day 7, the levels of inflammatory cytokines in the ME-Gel and MC-Gel groups were significantly reduced compared to the control group, but the MEMC-Gel group exhibited the lowest levels, showing the strongest anti-inflammatory effect. By day 14, the levels of inflammatory cytokines had generally decreased in all groups, but the MEMC-Gel group still showed significantly lower levels of TNF-α, IL-1β, and IL-6 than the other groups (Fig. 7C and D; Fig. S6). MEMC-Gel not only significantly inhibited the inflammatory response in the early phase, but also maintained its anti-inflammatory effects during the resolution phase. While both ME-Gel and MC-Gel effectively reduced the levels of inflammatory cytokines, MEMC-Gel demonstrated the most comprehensive anti-inflammatory effect. The sustained reduction in inflammatory cytokines, especially in the later stages of healing, suggests that MEMC-Gel can more effectively resist inflammation, which is essential for successful wound resolution and tissue regeneration. Additionally, we measured the levels of the anti-inflammatory cytokine IL-10 to assess the ability of each group to modulate the inflammatory environment at the wound. The results showed that on day 7, the IL-10 level in the MEMC-Gel group was significantly higher than in the other groups, suggesting that MEMC-Gel effectively promotes the expression of anti-inflammatory factors and enhances the anti-inflammatory response. By day 14, the IL-10 level in the MEMC-Gel group remained significantly higher than in the other groups, further confirming its superiority in terms of anti-inflammatory effects (Fig. 7E).

In summary, MEMC-Gel not only significantly reduced neutrophil infiltration but also significantly lowered the levels of key inflammatory cytokines (TNF-α, IL-1β, and IL-6) while increasing the expression of the anti-inflammatory cytokine IL-10. These results indicate that MEMC-Gel has a clear advantage in regulating the inflammatory response and promoting wound healing.

7 Antioxidant effects of MEMC-Gel in diabetic wounds

Diabetic wounds are often associated with severe oxidative stress, which not only delays the healing process but may also exacerbate the inflammatory response. Dihydroethidium (DHE) staining was performed on the wound tissues of mice, and the degree of oxidative damage was evaluated based on the intensity of the red fluorescence. Fluorescence results showed that, on days 7 and 14, the control group exhibited strong red fluorescence in the wound tissue, indicating a high level of oxidative stress. In contrast, the ME-Gel and MC-Gel groups showed reduced red fluorescence intensity (Fig. 8A), suggesting that these MSC-exo and MC-exo partially alleviated oxidative damage. However, the MEMC-Gel group exhibited a significant reduction in red fluorescence intensity, indicating that MEMC-Gel effectively suppressed the oxidative stress response. Further quantitative analysis revealed that the red fluorescence intensity in the MEMC-Gel group was significantly lower than that of the other groups on both days 7 and 14 (Fig. 8B). These results suggest that MEMC-Gel has strong antioxidant properties in diabetic wounds, effectively reducing oxidative stress levels and promoting wound healing.

Inhibition of hydroxyl radical (·OH) generation is critical for mitigating oxidative stress and facilitating wound healing. ·OH are highly reactive species generated during oxidative stress that can cause severe damage to cell membrane lipids, proteins, and DNA, thereby exacerbating inflammation and delaying tissue repair. To further verify the effect of MEMC-Gel in inhibiting ·OH, a commercial kit was used to measure the ·OH inhibition rate in the wound tissues of mice. In the ME-Gel and MC-Gel groups, the ·OH inhibition rates in the wound tissues were 71.74 ± 2.39 % and 65.34 ± 3.09 %, respectively, on day 14. This indicates that these treatments partially reduced ·OH production, thereby mitigating the adverse effects of oxidative stress on wound healing, with MSC-exo showing a slight advantage in inhibiting ·OH compared to MC-exo. In the MEMC-Gel group, the inhibition rate of ·OH was the most significant. On day 7, the ·OH inhibition rate in the MEMC-Gel group reached 63.26 ± 6.79 %, and by day 14, it further increased to 77.46 ± 4.48 % (Fig. 8C). This marked inhibition suggests that MEMC-Gel more effectively reduces ·OH generation, thereby significantly alleviating oxidative stress-induced damage in wound tissue. The enhanced ·OH inhibition observed with MEMC-Gel supports its superior role in mitigating oxidative damage, which is critical for the healing of diabetic wounds that are often characterized by excessive oxidative stress.

SOD, MDA, and glutathione (GSH) levels are key biomarkers reflecting the oxidative stress status of the body [62]. GSH is an important intracellular antioxidant that protects cells from oxidative damage by reducing free radicals and maintaining normal cellular functions. To further evaluate the effect of MEMC-Gel in inhibiting oxidative stress, we measured the levels of these biomarkers in the wound tissues of diabetic mice. Compared to the control group, the ME-Gel and MC-Gel groups showed increased SOD activity (Fig. 8D), decreased MDA levels (Fig. 8E), and increased GSH levels in the wound tissues (Fig. S7), but these changes were less pronounced than those observed in the MEMC-Gel group. These results suggest that MEMC-Gel significantly enhances SOD activity, reduces MDA levels, and increases GSH levels in the wound tissues of diabetic mice, effectively alleviating oxidative stress. The enhanced antioxidant enzyme activity and reduction in oxidative damage markers in the MEMC-Gel suggest its role in restoring the balance of the oxidative-antioxidative system in diabetic wound healing.

In conclusion, MEMC-Gel effectively reduces oxidative stress in diabetic wounds by significantly inhibiting hydroxyl radical generation and enhancing antioxidant defense mechanisms. This promotes wound healing by mitigating the detrimental effects of oxidative stress. Combined with its previously demonstrated anti-inflammatory effects, MEMC-Gel presents a powerful candidate for the treatment of diabetic wounds and holds significant potential for clinical application.

8 MEMC-Gel improves the microenvironment for wound healing in diabetic wounds

The application of MEMC-Gel in diabetic wounds not only counteracts the inflammatory response and significantly inhibits oxidative stress, but also improves the wound microenvironment through multiple mechanisms, thereby promoting wound healing. Macrophages, as key components of the immune system, play a crucial role in influencing the inflammatory response and repair process of wounds, with their polarization state being particularly important. The transition from pro-inflammatory M1 macrophages to anti-inflammatory and repair-oriented M2 macrophages helps alleviate inflammation and promotes tissue repair. To further investigate the effects of MEMC-Gel on macrophage polarization, IHC analysis was conducted. In the wound tissues of mice treated with MEMC-Gel, the expression of the pro-inflammatory M1 macrophage marker iNOS was significantly reduced (Fig. 9A), while the expression of the anti-inflammatory and repair-associated M2 macrophage marker CD206 was significantly increased (Fig. 9C). Quantitative analysis of iNOS and CD206 expression confirmed the regulatory effect of MEMC-Gel on macrophage polarization (Fig. 9B and D). On day 3, the MEMC-Gel group exhibited a

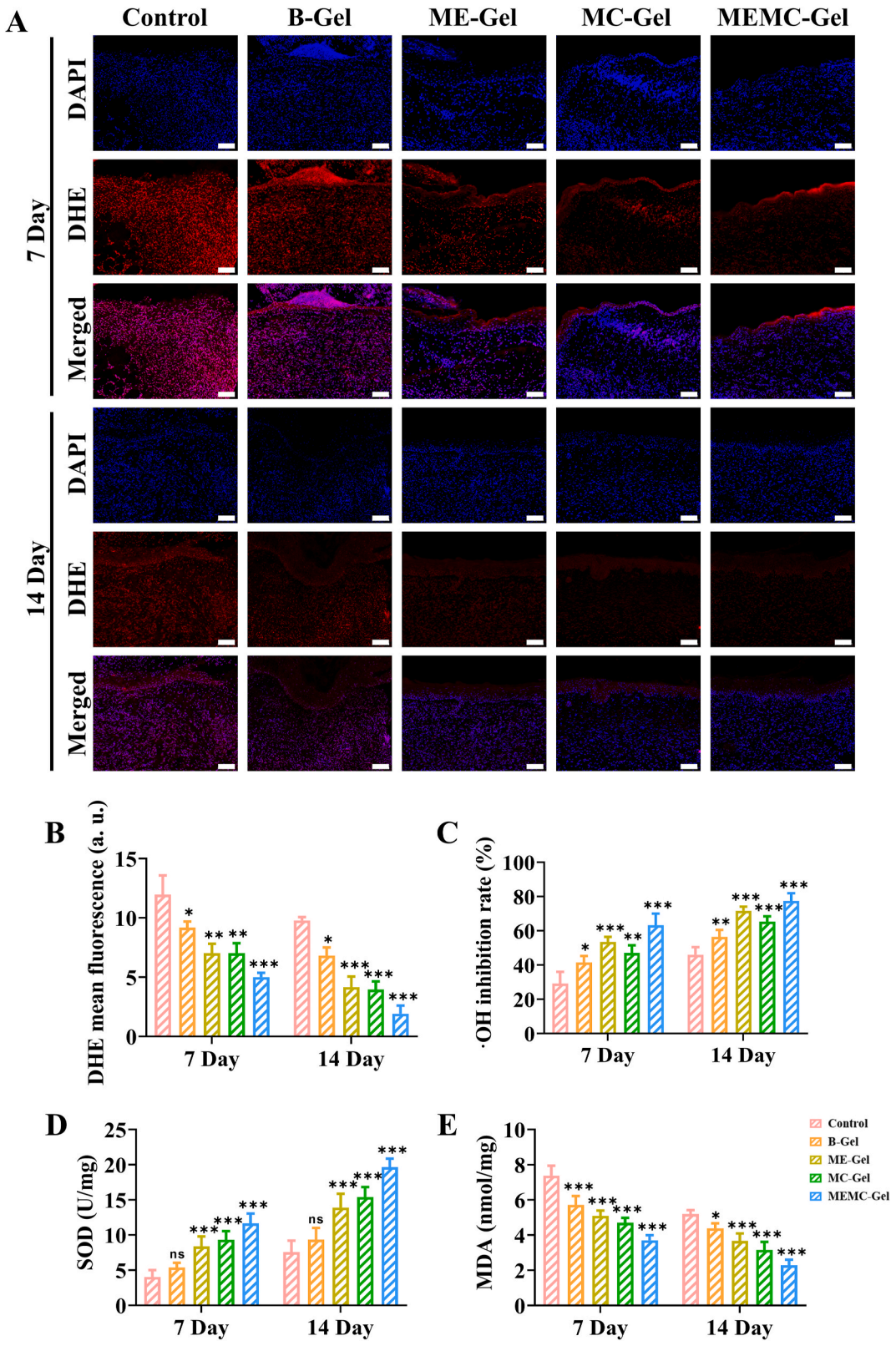

Fig. 8. Antioxidant effects of MEMC-Gel in animal experiments. (A). DHE fluorescence staining of wound tissue at different time points following various treatments. Scale bar is 100 μm. (B). Quantitative analysis of the fluorescence intensity of DHE (n = 3). Detection of antioxidant indicators in wound tissue at different time points following various treatments: (C) •OH, (D) SOD and (E) MDA (n = 5). All data are shown as the mean ± SD. Compared with control group, ns ≥ 0.05, *p < 0.05, **p < 0.01, ***p < 0.001.

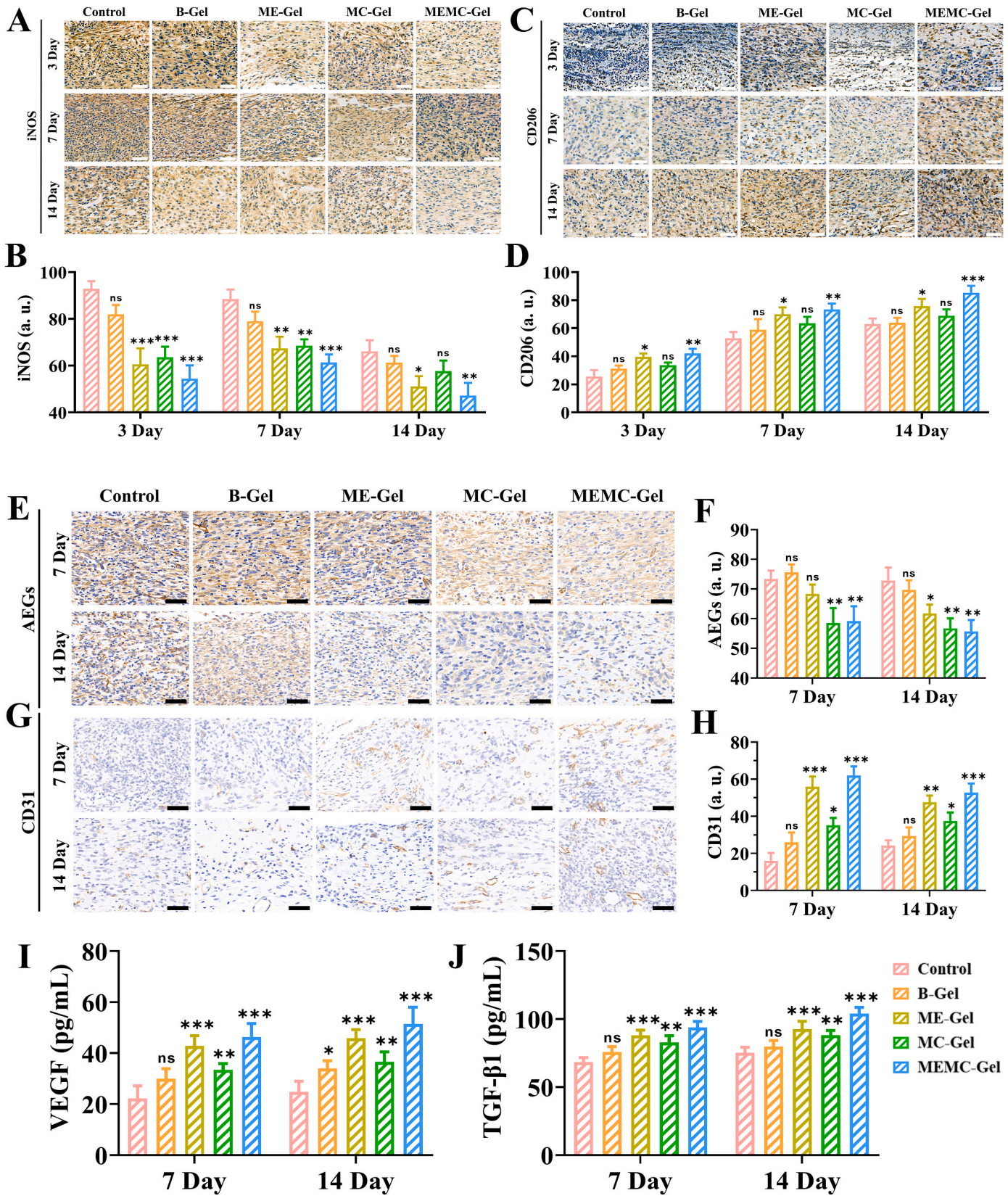

Fig. 9. Regulatory effects of MEMC-Gel on macrophages and pro-angiogenic activity in animal experiments. IHC staining of (A) iNOS, (C) CD206, (E) AEGs and (G) CD31 of wound tissue at different time points following various treatments. Scale bar is 50 μm. Quantitative analysis of (B) iNOS, (D) CD206, (F) AEGs and (H) CD31 expression of wound tissue (n = 3). ELISA detection of the levels of (I) TGF-β1 and (J) VEGF in wound tissue at different time points following various treatments (n = 5). All data are shown as the mean ± SD. Compared with control group, ns ≥ 0.05, *p < 0.05, **p < 0.01, ***p < 0.001.

significant reduction in iNOS positive cells, indicating strong initial suppression of pro-inflammatory M1 macrophages. By day 7, although iNOS expression decreased in the control group, it increased in the ME-Gel, MC-Gel, and MEMC-Gel groups compared to their previous levels but remained lower than in the control group. This indicates that MEMC-Gel can effectively reduce and delay the peak polarization of M1 macrophages. By day 14, iNOS expression further declined across all groups, with the MEMC-Gel group showing significantly lower levels of iNOS expression than the other groups. Conversely, the expression of CD206, a marker for anti-inflammatory M2 macrophages, slightly increased in the MEMC-Gel group from day 3, indicating an early shift toward an anti-inflammatory environment. By day 7, the number of CD206 positive cells further increased, and by day 14, CD206 expression remained at a high level in the MEMC-Gel group, highlighting the MEMC ability to sustain M2 macrophage activity. These data suggest that MEMC-Gel effectively inhibits the activity of pro-inflammatory M1 macrophages while promoting the proliferation and functional activation of anti-inflammatory and repair-oriented M2 macrophages. The temporal changes in M1 and M2 macrophage populations, with early suppression of M1 and sustained promotion of M2, underscore the potential of MEMC-Gel to manage inflammation and promote healing throughout the different phases of the wound healing process. These findings underscore the dual role of MEMC-Gel in both early and late stages of wound healing.

Hyperglycemia leads to persistent inflammation and increased oxidative stress, which can disrupt the normal healing process. To validate the hypoglycemic effect of MC-exo, we conducted an additional experiment. Diabetic mice were orally administered with MC-exo at a dose of 200 mg/kg, while the control group received an equal volume of PBS. The results showed that the fasting blood glucose levels in the MC group were significantly lower than those in the control group (Fig. S8). This hypoglycemic effect of MC-exo suggests its potential in improving the wound microenvironment by reducing hyperglycemia-induced oxidative stress and inflammation, thereby facilitating better wound healing. Under hyperglycemic conditions, the formation and accumulation of AGEs are significantly increased, resulting in changes to the wound microenvironment. IHC analysis of AGEs in the wound tissues revealed that the expression of AGEs in the MEMC-Gel group was significantly lower than in the control group (Fig. 9E). Further quantitative analysis showed that, on both days 7 and 14, the AGEs expression levels in the MEMC-Gel and MC-Gel groups were similar and significantly lower than those in the control group (Fig. 9F). This suggests that the reduction of AGEs accumulation in the wound tissue may be attributed to the MC-exo in the hydrogel. Therefore, MEMC-Gel effectively reduces the blood glucose level around the wound and decreases the accumulation of AGEs, optimizing the wound microenvironment.

Angiogenesis is critical for supplying the wound with necessary nutrients and oxygen. The expression of angiogenic factors can significantly improve blood supply to the wound and accelerate tissue repair and regeneration. Through CD31 IHC staining, it was observed that on day 7, the MEMC-Gel group exhibited the highest CD31-positive rate in the wound tissue compared to the control group (Fig. 9G). Further quantitative analysis indicated that the CD31-positive rate in the MEMC-Gel and ME-Gel groups were similar, suggesting that MSC-exo may play a primary role in promoting angiogenesis. In contrast, the control group had fewer CD31-positive vessels, indicating sparse angiogenesis. On day 14, the CD31-positive rate in all groups decreased, likely due to the transition of the wound into the vascular remodeling phase. However, the MEMC-Gel group still exhibited the highest CD31-positive rate (Fig. 9H), suggesting that MEMC-Gel may have a better long-term healing effect and potential for tissue function recovery. The ability of MEMC-Gel to sustain high levels of angiogenesis indicates its potential for promoting not just initial wound closure but also long-term tissue stability and function. In short, MEMC-Gel demonstrates excellent therapeutic effects in promoting angiogenesis and tissue reconstruction. Vascular endothelial growth factor (VEGF) and transforming growth factor β1 (TGF-β1) play key roles in the process of angiogenesis, particularly in the regulation of endothelial cell proliferation, migration, and lumen formation. On day 7, the VEGF content in the MEMC-Gel group was approximately 2.09 times higher than that of the control group (Fig. 9I), while TGF-β1 levels were about 1.37 times higher (Fig. 9J), indicating that MEMC-Gel significantly promotes the expression of angiogenesis-related factors during the early stages of wound healing. On day 14, although the differences in VEGF and TGF-β1 expression between the groups diminished, the MEMC-Gel group still exhibited significantly higher levels compared to the control group, further confirming its sustained effect in promoting angiogenesis and maturation. Additionally, the VEGF content in the ME-Gel group was significantly higher than that in the MC-Gel group, suggesting that MSC-exo may play a more prominent role in promoting angiogenesis. Notably, although both the ME-Gel and MC-Gel groups demonstrated good angiogenic effects, the MEMC-Gel group, by combining the advantages of both, exhibited more pronounced results. It not only rapidly increased the expression of angiogenic factors (VEGF and TGF-β1) during the early stage but also maintained a higher level in the later stage, promoting the maturation and stability of blood vessels. Overall, MEMC-Gel significantly enhanced the vascularization and tissue repair capacity of the wound. Its sustained effects in both the early and late stages suggest its long-term therapeutic potential in wound healing.

Through multiple mechanisms, MEMC-Gel effectively inhibits inflammation and oxidative stress, modulates macrophage polarization by reducing the number of pro-inflammatory M1 macrophages and increasing the number of anti-inflammatory and repair-oriented M2 macrophages, thereby optimizing the wound microenvironment. Furthermore, MEMC-Gel significantly reduces the accumulation of advanced glycation end products (AGEs), mitigating the adverse effects of hyperglycemia on wound healing. In terms of promoting angiogenesis, MEMC-Gel increased the number of CD31-positive blood vessels in the wound area and enhanced the expression of VEGF and TGF-β1, significantly promoting the formation and maturation of new blood vessels and improving the vascularization of the wound microenvironment. In conclusion, MEMC-Gel demonstrates remarkable therapeutic effects in diabetic wound healing.

9 The biocompatibility of MEMC-Gel in vivo

The in vivo biocompatibility of MEMC-Gel is a critical factor in assessing its clinical feasibility [63]. To comprehensively evaluate the biocompatibility of MEMC-Gel, hemolysis tests were first conducted. The results of the hemolysis assay showed that MEMC-Gel did not induce significant red blood cell lysis upon contact with blood (***Fig. S 9A***), with a hemolysis rate below 5 % (Fig. S 9B), demonstrating its excellent blood compatibility. Furthermore, MEMC-Gel was applied to the wounds of healthy mice, and one week later, their major organs (including the liver, kidney, heart, lungs, and spleen) were harvested for histological analysis using H&E staining. The staining results revealed no apparent pathological changes or morphological abnormalities in these organs following MEMC-Gel treatment compared to healthy mice (Fig. S 9C). The tissue architecture remained intact, with normal cell arrangement and no signs of inflammatory cell infiltration or tissue damage. The absence of pathological changes in major organs indicates that MEMC-Gel is biocompatible. These findings suggest that MEMC-Gel is safe for in vivo applications and does not cause harm to major organs. To sum up, MEMC-Gel exhibits excellent in vivo biocompatibility, with good blood compatibility and safety for major organs, providing a strong foundation for its clinical application in wound healing and tissue engineering.

4. Summary

In this study, we developed and characterized a novel in situ photo-crosslinked hydrogel, which simultaneously incorporates exosomes

derived from stem cells and plant sources as bioactive components for diabetic wound repair. Using GelMA and DA as the framework, this hydrogel was photo-crosslinked to encapsulate MSC-exo and MC-exo, successfully creating a multifunctional hydrogel. MEMC-Gel exhibits excellent mechanical properties, adhesion, and degradability, meeting the requirements for diabetic wound applications. Additionally, cell-based assays demonstrated the hydrogel remarkable biocompatibility, as well as its excellent ability to promote cell migration, angiogenesis, and provide antioxidant and anti-inflammatory effects, and regulate macrophage polarization. Animal experiments revealed that MEMC-Gel enhances wound healing by suppressing inflammation, combating oxidative stress, and modulating the immune response of macrophages in the wound microenvironment. It also improved the hyperglycemic condition in the wound microenvironment and promoted angiogenesis, ultimately improving wound repair. In conclusion, MEMC-Gel, through its synergistic multi-pathway actions, significantly accelerates the healing of diabetic wounds. This innovative bioactive dressing offers a promising new solution for diabetic wound repair and provides a novel therapeutic approach for the clinical treatment of chronic wound healing.

CRediT authorship contribution statement

Jialu Weng: Writing – original draft, Investigation. **Yizhang Chen:** Formal analysis. **Yuhan Zeng:** Validation. **Wenzhang Jin:** Writing – review & editing, Supervision, Methodology, Data curation. **Ying Ji:** Validation. **Wa Zhang:** Validation, Formal analysis. **Shunfu Wang:** Validation. **Haobing Li:** Formal analysis. **Meilin Yi:** Formal analysis. **Xiaoying Niu:** Visualization. **Xuchen Deng:** Validation. **Jiancheng Huang:** Conceptualization. **Xiang Su:** Resources, Funding acquisition. **Lulu Chen:** Resources, Funding acquisition, Conceptualization.

Ethics approval statement

All animal procedures in this experiment have been approved by the Ethics Committee of the First Affiliated Hospital of Wenzhou Medical University and the Animal Experimentation Ethics Committee of Zhejiang Province (Approval number: WYYY-IACUC-AEC-2025-014).

Permission to reproduce material from other sources

No.

Declaration of competing interest

The authors declare no potential conflicts of interest with respect to the research, authorship, and publication of this article.

Acknowledgments

This research was supported by Zhejiang Provincial Natural Science Foundation of China under Grant No. LQ22H290003.

Appendix A. Supplementary data

Supplementary data to this article can be found online at https://doi.org/10.1016/j.mtbio.2025.101810.

Data availability

Data will be made available on request.

References

[1] K. McDermott, M. Fang, A.J. Boulton, E. Selvin, C.W. Hicks, Etiology, epidemiology, and disparities in the burden of diabetic foot ulcers, Diabetes Care 46 (1) (2023) 209–221.
[2] L. Sun, Z. Wang, H. Kang, P. Luo, J. Su, W. Wei, P. Zhou, A. Yu, H. Dai, A flexibility self-powered Band-Aid for diabetes wound healing and skin bioelectronics, Chem. Eng. J. 481 (2024) 148096.
[3] L. Yang, F. Liang, X. Zhang, Y. Jiang, F. Duan, L. Li, F. Ren, Remodeling microenvironment based on MOFs-Hydrogel hybrid system for improving diabetic wound healing, Chem. Eng. J. 427 (2022) 131506.
[4] P. Wang, J. Wu, H. Yang, H. Liu, T. Yao, C. Liu, Y. Gong, M. Wang, G. Ji, P. Huang, Intelligent microneedle patch with prolonged local release of hydrogen and magnesium ions for diabetic wound healing, Bioact. Mater. 24 (2023) 463–476.
[5] E.A. Friedman, Advanced glycosylated end products and hyperglycemia in the pathogenesis of diabetic complications, Diabetes Care 22 (1999) B65.
[6] Q. Li, Y. Wen, L. Wang, B. Chen, J. Chen, H. Wang, L. Chen, Hyperglycemia-induced accumulation of advanced glycosylation end products in fibroblast-like synoviocytes promotes knee osteoarthritis, Exp. Mol. Med. 53 (11) (2021) 1735–1747.
[7] F. Giacco, M. Brownlee, Oxidative stress and diabetic complications, Circ. Res. 107 (9) (2010) 1058–1070.
[8] L. Deng, C. Du, P. Song, T. Chen, S. Rui, D.G. Armstrong, W. Deng, The role of oxidative stress and antioxidants in diabetic wound healing, Oxid. Med. Cell. Longev. 2021 (1) (2021) 8852759.
[9] J.M. Forbes, A.K. Fotheringham, Vascular complications in diabetes: old messages, new thoughts, Diabetologia 60 (2017) 2129–2138.
[10] D. Baltzis, I. Eleftheriadou, A. Veves, Pathogenesis and treatment of impaired wound healing in diabetes mellitus: new insights, Adv. Ther. 31 (2014) 817–836.
[11] F. Mohsin, S. Javaid, M. Tariq, M. Mustafa, Molecular immunological mechanisms of impaired wound healing in diabetic foot ulcers (DFU), current therapeutic strategies and future directions, Int. Immunopharmacol. 139 (2024) 112713.
[12] M.G. Monaghan, R. Borah, C. Thomsen, S. Browne, Thou shall not heal, Overcoming the non-healing behaviour of diabetic foot ulcers by engineering the inflammatory microenvironment, Adv. Drug Deliv. Rev. (2023) 115120.
[13] Y. Gong, P. Wang, R. Cao, J. Wu, H. Ji, M. Wang, C. Hu, P. Huang, X. Wang, Exudate absorbing and antimicrobial hydrogel integrated with multifunctional curcumin-loaded magnesium polyphenol network for facilitating burn wound healing, ACS Nano 17 (22) (2023) 22355–22370.
[14] M. Sharifiaghdam, E. Shaabani, R. Faridi-Majidi, S.C. De Smedt, K. Braeckmans, J. C. Fraire, Macrophages as a therapeutic target to promote diabetic wound healing, Mol. Ther. 30 (9) (2022) 2891–2908.
[15] A.S. Rayate, B.S. Nagoba, S.S. Mumbre, H.B. Mavani, A.M. Gavkare, A. S. Deshpande, Current scenario of traditional medicines in management of diabetic foot ulcers: a review, World J. Diabetes 14 (1) (2023) 1.
[16] R.F. Pereira, P.J. Bartolo, Traditional therapies for skin wound healing, Adv. Wound Care 5 (5) (2016) 208–229.
[17] J. Boateng, O. Catanzano, Advanced therapeutic dressings for effective wound healing—a review, J. Pharmaceut. Sci. 104 (11) (2015) 3653–3680.
[18] T. Zivari-Ghader, M.-R. Rashidi, M. Mehrali, Biological macromolecule-based hydrogels with antibacterial and antioxidant activities for wound dressing: a review, Int. J. Biol. Macromol. (2024) 134578.
[19] Y. Yang, S. Zhong, F. Meng, X. Cui, Multi-Functional hydrogels to promote diabetic wound Healing: a review, Chem. Eng. J. (2024) 154855.
[20] L. Long, W. Liu, C. Hu, L. Yang, Y. Wang, Construction of multifunctional wound dressings with their application in chronic wound treatment, Biomater. Sci. 10 (15) (2022) 4058–4076.
[21] R. Kalluri, V.S. LeBleu, The biology, function, and biomedical applications of exosomes, Science 367 (6478) (2020) eaau6977.
[22] J. Rezaie, S. Ajezi, Ç.B. Avci, M. Karimipour, M.H. Geranmayeh, A. Nourazarian, E. Sokullu, A. Rezabakhsh, R. Rahbarghazi, Exosomes and their application in biomedical field: difficulties and advantages, Mol. Neurobiol. 55 (2018) 3372–3393.
[23] S. Kim, Y. Kim, Y.-S. Hyun, H. Choi, S.-Y. Kim, T.-G. Kim, Exosomes from human cord blood plasma accelerate cutaneous wound healing by promoting fibroblast function, angiogenesis, and M2 macrophage differentiation, Biomater. Sci. 9 (8) (2021) 3028–3039.
[24] X. Teng, T. Liu, G. Zhao, Y. Liang, P. Li, F. Li, Q. Li, J. Fu, C. Zhong, X. Zou, A novel exosome-based multifunctional nanocomposite platform driven by photothermal-controlled release system for repair of skin injury, J. Contr. Release 371 (2024) 258–272.
[25] D. Bian, Y. Wu, G. Song, R. Azizi, A. Zamani, The application of mesenchymal stromal cells (MSCs) and their derivative exosome in skin wound healing: a comprehensive review, Stem Cell Res. Ther. 13 (1) (2022) 24.
[26] C. Zhou, B. Zhang, Y. Yang, Q. Jiang, T. Li, J. Gong, H. Tang, Q. Zhang, Stem cell-derived exosomes: emerging therapeutic opportunities for wound healing, Stem Cell Res. Ther. 14 (1) (2023) 107.
[27] H. Ma, W.-S. Siu, P.-C. Leung, The potential of MSC-based cell-free therapy in wound healing—a thorough literature review, Int. J. Mol. Sci. 24 (11) (2023) 9356.
[28] S. Madhan, R. Dhar, A. Devi, Plant-derived exosomes: a green approach for cancer drug delivery, J. Mater. Chem. B 12 (9) (2024) 2236–2252.
[29] M. Nemati, B. Singh, R.A. Mir, M. Nemati, A. Babaei, M. Ahmadi, Y. Rasmi, A. G. Golezani, J. Rezaie, Plant-derived extracellular vesicles: a novel nanomedicine approach with advantages and challenges, Cell Commun. Signal. 20 (1) (2022) 69.

[30] X. Zhang, L. Zhang, B. Zhang, K. Liu, J. Sun, Q. Li, L. Zhao, Herbal tea, a novel adjuvant therapy for treating type 2 diabetes mellitus: a review, Front. Pharmacol. 13 (2022) 982387.
[31] B.C. Panda, S. Mondal, K.S.P. Devi, T.K. Maiti, S. Khatua, K. Acharya, S.S. Islam, Pectic polysaccharide from the green fruits of Momordica charantia (Karela): structural characterization and study of immunoenhancing and antioxidant properties, Carbohydr. Res. 401 (2015) 24–31.
[32] R. Singh, I. Garcia-Gomez, K.P. Gudehithlu, A.K. Singh, Bitter melon extract promotes granulation tissue growth and angiogenesis in the diabetic wound, Adv. Skin Wound Care 30 (1) (2017) 16–26.
[33] M. Raish, Momordica charantia polysaccharides ameliorate oxidative stress, hyperlipidemia, inflammation, and apoptosis during myocardial infarction by inhibiting the NF-κB signaling pathway, Int. J. Biol. Macromol. 97 (2017) 544–551.
[34] P. Chaturvedi, Antidiabetic potentials of Momordica charantia: multiple mechanisms behind the effects, J. Med. Food 15 (2) (2012) 101–107.
[35] W. Nkambo, N.G. Anyama, B. Onegi, In vivo hypoglycemic effect of methanolic fruit extract of Momordica charantia L, Afr. Health Sci. 13 (4) (2013) 933–939.
[36] M. Cortez-Navarrete, E. Martínez-Abundis, K.G. Pérez-Rubio, M. González-Ortiz, M. Méndez-del Villar, Momordica charantia administration improves insulin secretion in type 2 diabetes mellitus, J. Med. Food 21 (7) (2018) 672–677.
[37] P. Kumari, R. Verma, G. Nayik, S. Solankey, Antioxidant potential and health benefits of Bitter gourd (Momordica charantia L.), J. Postharvest Technol 5 (2017) 1–8.
[38] Y. Liang, J. He, B. Guo, Functional hydrogels as wound dressing to enhance wound healing, ACS Nano 15 (8) (2021) 12687–12722.
[39] S. Xiao, T. Zhao, J. Wang, C. Wang, J. Du, L. Ying, J. Lin, C. Zhang, W. Hu, L. Wang, Gelatin methacrylate (GelMA)-based hydrogels for cell transplantation: an effective strategy for tissue engineering, Stem cell Rev. Rep. 15 (2019) 664–679.
[40] Z. Yang, R. Huang, B. Zheng, W. Guo, C. Li, W. He, Y. Wei, Y. Du, H. Wang, D. Wu, Highly stretchable, adhesive, biocompatible, and antibacterial hydrogel dressings for wound healing, Adv. Sci. 8 (8) (2021) 2003627.
[41] W. Jin, S. Shen, X. Xu, X. Xie, X. Zhou, X. Su, L. Wu, S. Wang, L. Zhang, B. Chen, All-in-one hydrogel patches with sprayed bFGF-loaded GelMA microspheres for infected wound healing studies, Int. J. Pharm. 658 (2024) 124205.
[42] A. Akbari, N. Jabbari, R. Sharifi, M. Ahmadi, A. Vahhabi, S.J. Seyedzadeh, M. Nawaz, S. Szafert, M. Mahmoodi, E. Jabbari, Free and hydrogel encapsulated exosome-based therapies in regenerative medicine, Life Sci. 249 (2020) 117447.
[43] J. Gan, L. Sun, G. Chen, W. Ma, Y. Zhao, L. Sun, Mesenchymal stem cell exosomes encapsulated oral microcapsules for acute colitis treatment, Adv. Healthcare Mater. 11 (17) (2022) 2201105.
[44] W.-W. Cui, C. Ye, K.-X. Wang, X. Yang, P.-Y. Zhu, K. Hu, T. Lan, L.-Y. Huang, W. Wang, B. Gu, Momordica. charantia-derived extracellular vesicles-like nanovesicles protect cardiomyocytes against radiation injury via attenuating DNA damage and mitochondria dysfunction, Front. Cardiovasc. Med. 9 (2022) 864188.
[45] S. Tan, Z. Liu, M. Cong, X. Zhong, Y. Mao, M. Fan, F. Jiao, H. Qiao, Dandelion-derived vesicles-laden hydrogel dressings capable of neutralizing Staphylococcus aureus exotoxins for the care of invasive wounds, J. Contr. Release 368 (2024) 355–371.
[46] M. Yuan, K. Liu, T. Jiang, S. Li, J. Chen, Z. Wu, W. Li, R. Tan, W. Wei, X. Yang, GelMA/PEGDA microneedles patch loaded with HUVECs-derived exosomes and Tazarotene promote diabetic wound healing, J. Nanobiotechnol. 20 (1) (2022) 147.
[47] N. Xu, Y. Gao, Z. Li, Y. Chen, M. Liu, J. Jia, R. Zeng, G. Luo, J. Li, Y. Yu, Immunoregulatory hydrogel decorated with Tannic acid/Ferric ion accelerates diabetic wound healing via regulating Macrophage polarization, Chem. Eng. J. 466 (2023) 143173.
[48] S. Nath, S.K. Ghosh, Y. Choudhury, A murine model of type 2 diabetes mellitus developed using a combination of high fat diet and multiple low doses of streptozotocin treatment mimics the metabolic characteristics of type 2 diabetes mellitus in humans, J. Pharmacol. Toxicol. Methods 84 (2017) 20–30.
[49] M. Zhang, X.-Y. Lv, J. Li, Z.-G. Xu, L. Chen, The characterization of high-fat diet and multiple low-dose streptozotocin induced type 2 diabetes rat model, Exp. Diabetes Res. 2008 (2008).
[50] V.S. Chernyshev, R. Rachamadugu, Y.H. Tseng, D.M. Belnap, Y. Jia, K.J. Branch, A. E. Butterfield, L.F. Pease, P.S. Bernard, M. Skliar, Size and shape characterization of hydrated and desiccated exosomes, Anal. Bioanal. Chem. 407 (2015) 3285–3301.
[51] N. Zhang, N. Sun, C. Deng, Rapid isolation and proteome analysis of urinary exosome based on double interactions of Fe3O4@ TiO2-DNA aptamer, Talanta 221 (2021) 121571.
[52] T.L. Ramos, L.I. Sánchez-Abarca, S. Muntión, S. Preciado, N. Puig, G. López-Ruano, Á. Hernández-Hernández, A. Redondo, R. Ortega, C. Rodríguez, MSC surface markers (CD44, CD73, and CD90) can identify human MSC-derived extracellular vesicles by conventional flow cytometry, Cell Commun. Signal. 14 (2016) 1–14.
[53] M. Pinedo, L. de la Canal, C. de Marcos Lousa, A call for Rigor and standardization in plant extracellular vesicle research, J. Extracell. Vesicles 10 (6) (2021) e12048.
[54] X. Ou, H. Wang, H. Tie, J. Liao, Y. Luo, W. Huang, R. Yu, L. Song, J. Zhu, Novel plant-derived exosome-like nanovesicles from Catharanthus roseus: preparation, characterization, and immunostimulatory effect via TNF-α/NF-κB/PU. 1 axis, J. Nanobiotechnol. 21 (1) (2023) 160.
[55] C. Xie, X. Wang, H. He, Y. Ding, X. Lu, Mussel-inspired hydrogels for self-adhesive bioelectronics, Adv. Funct. Mater. 30 (25) (2020) 1909954.
[56] M. Guvendiren, H.D. Lu, J.A. Burdick, Shear-thinning hydrogels for biomedical applications, Soft Matter 8 (2) (2012) 260–272.
[57] P. Jain, H. Kathuria, N. Dubey, Advances in 3D bioprinting of tissues/organs for regenerative medicine and in-vitro models, Biomaterials 287 (2022) 121639.
[58] A.V.P. Bobadilla, J. Arévalo, E. Sarró, H.M. Byrne, P.K. Maini, T. Carraro, S. Balocco, A. Meseguer, T. Alarcón, In vitro cell migration quantification method for scratch assays, J. R. Soc. Interface 16 (151) (2019) 20180709.
[59] F. Yang, Y. Qiu, X. Xie, X. Zhou, S. Wang, J. Weng, L. Wu, Y. Ma, Z. Wang, W. Jin, Platelet membrane-encapsulated poly (lactic-co-glycolic acid) nanoparticles loaded with sildenafil for targeted therapy of vein graft intimal hyperplasia, Int. J. Pharm. X 8 (2024) 100278.
[60] W. Jin, X. Xie, S. Shen, X. Zhou, S. Wang, L. Zhang, X. Su, Ultrasmall polyvinylpyrrolidone-modified iridium nanoparticles with antioxidant and anti-inflammatory activity for acute pancreatitis alleviation, J. Biomed. Mater. Res. 112 (7) (2024) 988–1003.
[61] Y. Aratani, Myeloperoxidase: its role for host defense, inflammation, and neutrophil function, Arch. Biochem. Biophys. 640 (2018) 47–52.
[62] I. Marrocco, F. Altieri, I. Peluso, Measurement and clinical significance of biomarkers of oxidative stress in humans, Oxid. Med. Cell. Longev. 2017 (1) (2017) 6501046.
[63] Z. Wang, Y. Long, J. Fan, C. Xiao, C. Tong, C. Guo, X. Chen, B. Liu, X. Yang, Biosafety and biocompatibility assessment of Prussian blue nanoparticles in vitro and in vivo, Nanomedicine 15 (27) (2020) 2655–2670.